

UC Berkeley

UC Berkeley Previously Published Works

Title

Evaluating temporal controls on greenhouse gas (GHG) fluxes in an Arctic tundra environment: An entropy-based approach

Permalink

<https://escholarship.org/uc/item/4w411602>

Authors

Arora, Bhavna

Wainwright, Haruko M

Dwivedi, Dipankar

et al.

Publication Date

2019-02-01

DOI

10.1016/j.scitotenv.2018.08.251

Peer reviewed

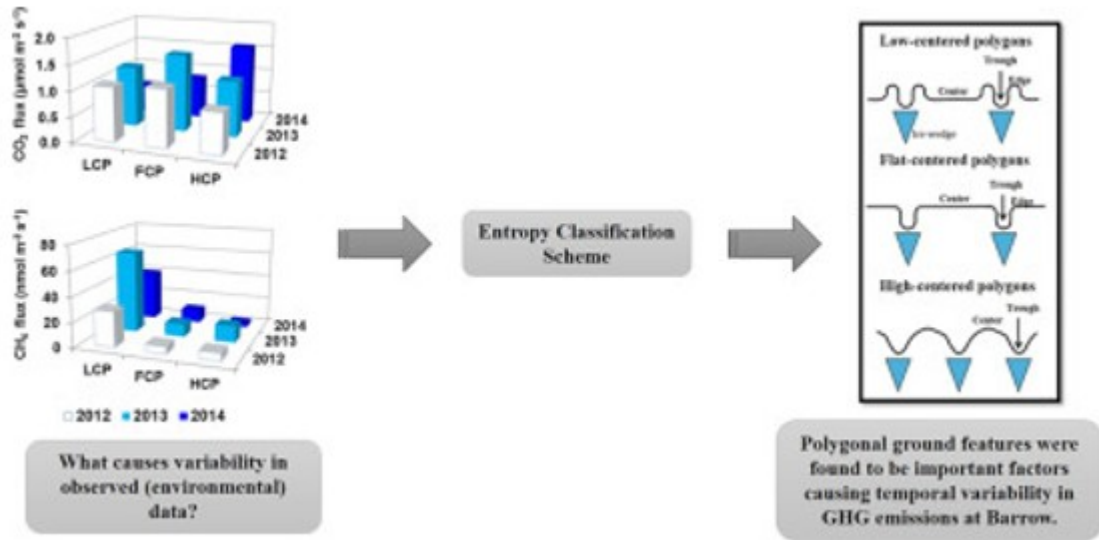
# Evaluating temporal controls on greenhouse gas (GHG) fluxes in an Arctic tundra environment: An entropy-based approach

Bhavna Arora<sup>a</sup> Haruko M. Wainwright<sup>a</sup> Dipankar Dwivedi<sup>a</sup> Lydia J.S. Vaughn<sup>a</sup>  
John B. Curtis<sup>b</sup> Margaret S. Torn<sup>a</sup> Baptiste Dafflon<sup>a</sup> Susan S. Hubbard<sup>a</sup>

## Abstract

There is significant spatial and temporal variability associated with greenhouse gas (GHG) fluxes in high-latitude Arctic tundra environments. The objectives of this study are to investigate temporal variability in CO<sub>2</sub> and CH<sub>4</sub> fluxes at Barrow, AK and to determine the factors causing this variability using a novel entropy-based classification scheme. In particular, we analyzed which geomorphic, soil, vegetation and climatic properties most explained the variability in GHG fluxes (opaque chamber measurements) during the growing season over three successive years. Results indicate that multi-year variability in CO<sub>2</sub> fluxes was primarily associated with soil temperature variability as well as vegetation dynamics during the early and late growing season. Temporal variability in CH<sub>4</sub> fluxes was primarily associated with changes in vegetation during the growing season and its interactions with primary controls like seasonal thaw. Polygonal ground features, which are common to Arctic regions, also demonstrated significant multi-year variability in GHG fluxes. Our results can be used to prioritize field sampling strategies, with an emphasis on measurements collected at locations and times that explain the most variability in GHG fluxes. For example, we found that sampling primary environmental controls at the centers of high centered polygons in the month of September (when freeze-back period begins) can provide significant constraints on GHG flux variability - a requirement for accurately predicting future changes to GHG fluxes. Overall, entropy results document the impact of changing environmental conditions (e.g., warming, growing season length) on GHG fluxes, thus providing clues concerning the manner in which ecosystem properties may be shifted regionally in a future climate.

Graphical abstract



Keywords: CO<sub>2</sub> fluxes, CH<sub>4</sub> fluxes, Polygonal tundra, Climate change

## 1. Introduction

Identifying key factors causing temporal variability in CO<sub>2</sub> and CH<sub>4</sub> fluxes has been the subject of considerable research over the past two decades (e.g., Arora et al., 2016b; Bousquet et al., 2006; Janssens et al., 2001; Schimel et al., 2001). Temporal variability in carbon fluxes has been linked to environmental factors such as snowmelt timing, growing season dynamics, water table variations and temperature fluctuations (e.g., Arora et al., 2013; Grant et al., 2017; Yabusaki et al., 2017). In particular, Zona et al. (2009) showed that CH<sub>4</sub> fluxes in the growing season were strongly correlated with soil temperature and non-linearly correlated with water table depth. Harper et al. (2005) showed that decreasing the amount and increasing the timing between rainfall events decreased CO<sub>2</sub> fluxes over four growing seasons (1998–2001). Changes in plant productivity have also been correlated with seasonal and annual variability in carbon fluxes (Janssens et al., 2001; Street et al., 2007).

While several drivers of temporal variability in GHG fluxes have been identified, the relationship between GHG fluxes and these drivers shows considerable variability in space and time, thereby contributing to significant uncertainties in estimating future changes to landscape-level carbon budgets. For example, Friberg et al. (2000) indicated that CH<sub>4</sub> fluxes were related to soil temperature and water table in the late part of the summer, whereas the thickness of the thaw layer was the most important control in the early part of the season. Similarly, Grogan and Chapin III (1999) indicated that climate (temperature) had strong effects on belowground CO<sub>2</sub> release in both summer and winter seasons while the type of vegetation only impacted summer CO<sub>2</sub> efflux. Contrary to these findings, a separate study by Bubier et al. (2003) suggested that the effect of vegetation type on growing season CO<sub>2</sub> efflux varied significantly between wet and dry years. Together,

these studies suggest that different environmental factors can become important under different spatio-temporal settings. Moreover, recent studies have shown that temporal variability in environmental constraints may itself be unknown or masked by other variables. For example, Malhotra and Roulet (2015) showed that temperature sensitivity of CH<sub>4</sub> increased with increasing thaw, but this trend was not found to be consistent and suggested confounding effects of substrate or water limitation on the apparent temperature sensitivity. It is thus important to understand the mechanistic and site-specific nature of relationships between greenhouse gas fluxes and environmental factors, and quantitatively attribute temporal variability to specific factors at a given site.

Understanding the variable nature of relationships between GHG fluxes and environmental factors is particularly important in Arctic tundra environments because of the vast amount of soil carbon stored in these regions and the potential of these regions to convert from a global carbon sink to a source under warmer conditions (Billings et al., 1982; Oechel et al., 2000; Sistla et al., 2013). These relationships can be especially complex and difficult to interpret in Arctic environments because shifts in the timing of snowmelt and plant phenology can strongly influence CH<sub>4</sub> and CO<sub>2</sub> fluxes. For example, Mastepanov et al. (2013) showed that the differences in growing season CH<sub>4</sub> fluxes over 2006–2010 could not be explained by corresponding changes in driving factors like soil temperature or moisture. Instead, they found increases in CH<sub>4</sub> fluxes to be related to the date of snowmelt and recommended using the first day of snowmelt as a proxy for the start of the growing season. Raz-Yaseef et al. (2017) linked spring observations of carbon fluxes at a site in Barrow, Alaska (the same site as this study) to the delayed release of biogenic gas production from the previous fall season. Other studies have suggested that the onset and length of the growing season may be shifted by several days in higher latitudes, which can explain some of the variability observed in greenhouse gas fluxes in these regions (Liston et al., 2002; Stow et al., 2004; Tucker et al., 2001).

Temporal variability in GHG fluxes and their relationship to different drivers can be described by simple descriptive statistics (e.g., range, standard deviation, coefficient of variation) or advanced statistical methods (e.g., principal component analysis, K-means clustering) (e.g., Arora and Mohanty, 2017; Dwivedi et al., 2013, Dwivedi et al., 2016). However, simple descriptive statistics have limited use as different environmental factors may demonstrate a number of identical descriptive statistical properties (Matejka and Fitzmaurice, 2017). Moreover, other statistical methods (e.g., correlation analysis, K-means clustering, principal components analysis) typically work under the assumptions of normality or describe linear relationships between variables. Investigating the degree to which environmental factors can impact GHG fluxes in Arctic tundra environments thus requires an integrated approach that can take into account the temporal shifts and complex spatial interactions between predictor and response variables. In this context,

entropy methods have proven to be useful in determining the relative contributions of hydrologic interactions, vegetation structure, spatial zonation and other environmental factors to system dynamics (Arora et al., 2016a; Brunsell and Wilson, 2013; Dwivedi and Mohanty, 2016; Ruddell et al., 2013). Moreover, considering the fact that environmental data are naturally stochastic and nonlinear (Reimann and Filzmoser, 2000), we chose to employ trans-information – a nonlinear entropy technique – to extract dependencies between GHG fluxes and environmental variables. Trans-information is defined as a measure of the amount of information that one random variable (e.g., a primary environmental control like soil temperature) contains or explains about another random variable (e.g., GHG fluxes). The main advantage of using trans-information over other techniques is that it is a non-parametric approach that can integrate complex, multivariate datasets without making assumptions regarding the nature of functional dependencies implicit in these datasets (Arora et al., 2016a; Costa et al., 2002). Identifying these dependencies can be particularly useful for developing upscaling strategies, closing the gap with field observations as well as improving the representation of soil carbon stocks and their response to climate change in community land models. In addition, several studies have emphasized the power and strength of trans-information and entropy-based analyses in comparison to other commonly-used statistical approaches such as correlation analysis and classification methods (e.g., Battiti, 1994; Mogheir et al., 2004; Strehl et al., 2000). Considering these advantages, we use a novel classification scheme (described in more detail below) that uses trans-information to disentangle the complex relationships between environmental variables and GHG fluxes under different spatio-temporal settings.

The objectives of this study are to characterize temporal variability in CO<sub>2</sub> and CH<sub>4</sub> fluxes and investigate possible controls of such variations at a high-Arctic location near Barrow, Alaska using a novel entropy-based classification scheme. To reach these objectives, we chose a set of topographic locations across the site where we have measurements of soil, vegetation and climate parameters as well as greenhouse gas fluxes during three growing seasons (2012–2014). The remainder of this paper is organized as follows. Section 2 describes the Barrow field site, lists a set of potential factors that may impact GHG flux variations based on previous site investigations, and documents field datasets and observations available for the entropy analysis. Details of the entropy-based classification scheme are provided in Section 3. Section 4 presents the entropy analysis results for CO<sub>2</sub> and CH<sub>4</sub> fluxes and an example for extending the use of the classification scheme to other variables of interest. A summary of the important findings is provided in Section 5.

## 2. Study site and datasets

### 2.1. Site description

Our study site is located within the Barrow Environmental Observatory (BEO) (71.3°N, 156.61°E) in Arctic Alaska (Fig. 1a). The study site in Barrow, AK has been the subject of intensive investigation of climate change impacts on ecosystem processes as part of the Department of Energy's (DOE) Next Generation Ecosystem Experiments (NGEE-Arctic) project. Although comprehensive descriptions of the NGEE-Arctic “Barrow” site can be found elsewhere (Hubbard et al., 2013; Liljedahl et al., 2012, Liljedahl et al., 2011), we will briefly summarize the environmental conditions of the site for completeness.

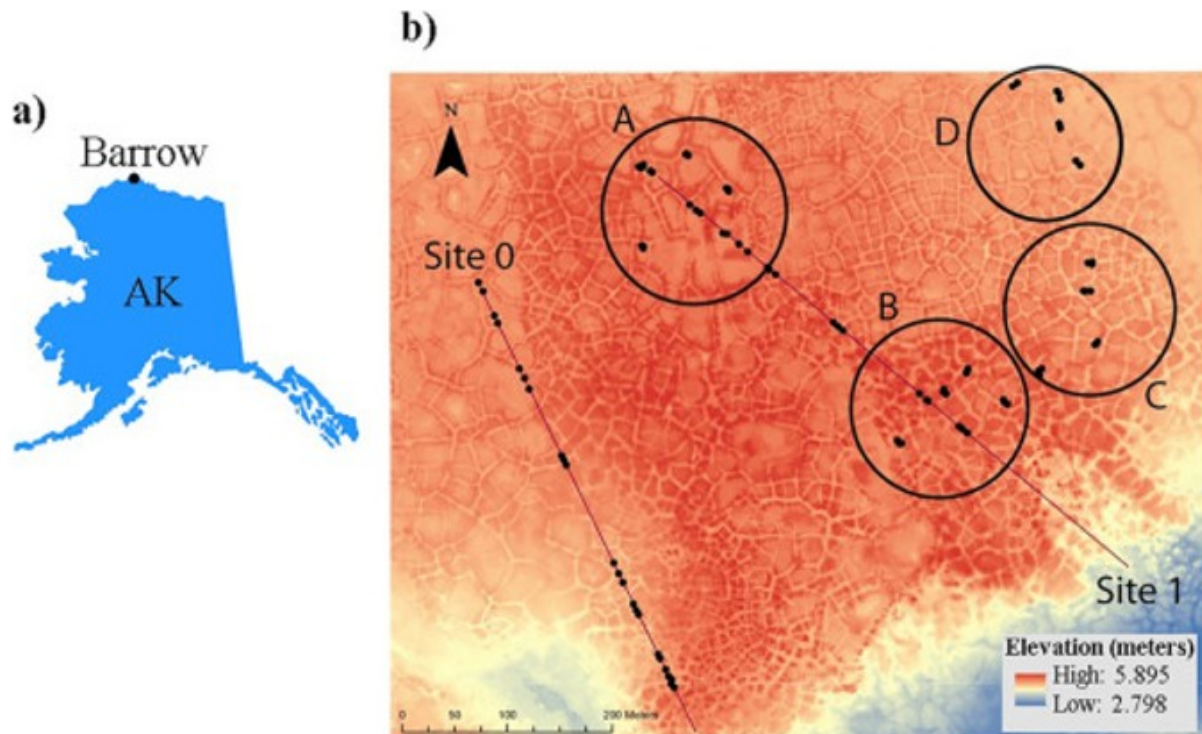


Fig. 1. a) Location of Barrow, Alaska, USA; b) LiDAR-based elevation map showing the locations of the intensive site 0 and site 1 transects (solid lines), A-D plots (open circles) as well as the automatic chamber stations (closed circles); and c) Schematic of different polygon types and features (modified from Wainwright et al., 2015). Details of the data collection efforts are presented in more detail elsewhere (Hubbard et al., 2013; Torn et al., 2013).

The landscape of the Barrow Peninsula is characterized by thaw lakes, drained thaw-lake basins (DTLB) and ice-wedge polygonal tundra (Hinkel and Nelson, 2003; Lara et al., 2015). The region has mostly continuous permafrost with thickness greater than 350 m at some locations (Sellman et al., 1975), and thaw depth varying between 20 and 70 cm (Shiklomanov et al., 2010). According to the DTLB classification by Hinkel et al. (2003), the majority of the Barrow site is located in the interstitial tundra, where ice-wedge polygons are prevalent. Ice-wedge polygons are initiated by the frost cracks of the ground due to extreme cold temperature. The growth of ice within the cracks creates wedge-shaped ice in the ground after repeated infiltration of water and freeze-expansion processes (Leffingwell, 1915; MacKay, 2000). Depending on the growth or degradation state of the ice

wedges, the polygons can be characterized as high-, flat- or low-centered (Fig. 1c) (MacKay, 2000). In particular, low-centered polygons have low, wet centers bordered by well-defined, topographically higher and dryer edges; high-centered polygons have topographically higher, well-drained centers and no clearly raised edges; while flat-centered polygons have an intermediate relief between high- and low-centered polygons (Vaughn et al., 2016).

Climate at the Barrow site is generally representative of wet coastal tundra regions. The mean annual air temperature and annual precipitation (1901–2007) at the site are  $-12\text{ }^{\circ}\text{C}$  and 113.5 mm, respectively (Hubbard et al., 2013). Precipitation occurs in the form of rainfall between June and September, with a maximum in August. Snowmelt usually occurs in late May to early June and freeze-up occurs in late September to October (Sturtevant et al., 2012). Vegetation at the site consists primarily of mosses, lichens and vascular plants such as *Carex aquatilis* and *Eriophorum* sp.

## 2.2. Factors regulating GHG fluxes at the site

Multiple factors potentially contribute to the temporal variability observed in GHG fluxes at the Barrow Site. Based on knowledge from previous investigations at the site, this study considers the following factors:

- **Geomorphology:** The geomorphology of the Barrow site is dominated by ice-wedge polygons, as indicated above. Several studies have shown that polygon-based microtopography can have a significant impact on water distribution and storage across the Arctic landscape (Engstrom et al., 2005; Helbig et al., 2013; Liljedahl et al., 2012; Minke et al., 2009). In particular, high-centered polygons represent a well-drained laterally-connected trough network (Liljedahl et al., 2016). In contrast, low-centered polygons decrease lateral connectivity and release storage water later in the summer as soil thaw progresses and opens new subsurface flow paths. These differences in microtopography and lateral drainage at the landscape-level can in turn influence plant distribution, microbial respiration, soil redox conditions, and consequently GHG fluxes. For example, Newman et al. (2015) documented significant variability in geochemical concentrations such as  $\text{Fe}^{2+}$ ,  $\text{NO}_3^-$ , and  $\text{PO}_4^{3-}$  across polygon types and features that can potentially impact GHG dynamics at the site. In addition, investigations conducted at Barrow have highlighted the co-variability of below-ground properties such as active layer depth, salinity distribution and permafrost conditions with polygon-based microtopography (Dafflon et al., 2016; Gangodagamage et al., 2014; Hubbard et al., 2013). Past investigations have also taken advantage of the unique property suites associated with different polygon types to identify ‘functional zones’ and their relationship to effective carbon flux (Wainwright et al., 2015). Because of the documented influence of geomorphic features on properties that influence carbon cycling at the Barrow site, we consider polygon types (low, high, or flat) and features (polygon center, edge, or

trough) as factors that also influence the GHG temporal fluxes in our entropy-based analysis.

- **Vegetation:** At the Barrow site, lower elevation areas (with higher water table) are occupied by vascular plants, particularly the graminoids *Carex aquatilis* and *Eriophorum* sp. (Sturtevant et al., 2012; Zona et al., 2011). In contrast, mosses (mainly *Sphagnum* sp.) and lichens dominate the higher elevation areas, with lower water table. Note that graminoids are known for transporting CH<sub>4</sub> via roots and stems such that CH<sub>4</sub> emissions have been correlated with vascular plant cover, sedge height and root density (Davidson et al., 2016; Sturtevant et al., 2012; von Fischer et al., 2010). Standing water is frequently observed at the site, which can confer a competitive advantage to graminoid productivity as compared to mosses (Grant et al., 2017) and thereby further increase CH<sub>4</sub> emissions. Ebullitive and diffusive fluxes from standing water can also contribute to methane emissions (Bastviken et al., 2004; Walter et al., 2007). In contrast, CO<sub>2</sub> emissions are typically expected to decrease in inundated conditions, but the response also depends on thaw conditions, hydrological connectivity and plant biomass (Grant et al., 2017; Mauritz et al., 2017).
- **Soil characteristics:** At Barrow, Oberbauer et al. (2007) showed that a standard warming treatment (rise in mean air temperature by 1–2 °C) using small open chambers increased net CO<sub>2</sub> uptake in wet regions but increased losses from dry regions. Model simulations further indicated that CO<sub>2</sub> and CH<sub>4</sub> emissions are strongly controlled by permafrost thaw and soil moisture gradients (Lawrence et al., 2015). We therefore considered several soil physical and thermal properties as potential controls on GHG fluxes.
- **Climatic conditions:** Climate has long been recognized as an important driver of GHG fluxes. For the Barrow site, several lines of evidence indicate that the mean annual air temperatures have increased by approximately 3 °C since 1950 (Chapin et al., 2005; IPCC, 2013; Lachenbruch and Marshall, 1986). Warmer air temperatures in Barrow may act to increase the thickness of soil that thaws on an annual basis, and the potential for further GHG release into the atmosphere (Atchley et al., 2016; Harp et al., 2016; Oechel et al., 1995). Moreover, studies have used temperature records and satellite data (normalized difference vegetation index) to suggest the lengthening of the growing season in high latitude Arctic regions (Myneni et al., 1997; Sharratt, 1992). More recently, Zona et al. (2016) suggested that soil temperatures were poised near 0 °C for more than 90 days in wetter regions of Barrow resulting in strong CH<sub>4</sub> emissions beyond the conventional growing season.
- **Temporal dynamics:** GHG fluxes are likely to be highly heterogeneous and dependent on many factors at the Barrow site. The goal of this study is to understand temporal variability in GHG fluxes in the presence of interactions and feedbacks amongst the many primary controls. For example, a recent study by Dafflon et al. (2017) has documented the increase in correlation



between vegetation greenness and thaw layer electrical measurements (a proxy for soil moisture and temperature) over the growing season, highlighting the covariability of vegetation and soil properties. The strength of this correlation was also found to be annually variable.

While Barrow has been the subject of several previous site investigations, these studies have focused mostly on a single year of GHG dynamics and/or analyzed topographic positions as the dominant control on variability. Although Dafflon et al. (2017) incorporated two years of autonomous measurements from electrical resistivity tomography, vegetation indices from a few weeks of optical camera operation, and other autonomous and manual point measurements, they did not include GHG flux dynamics in their study. Instead, their work was focused on quantifying the covariability of active layer depth, soil properties and vegetation dynamics using geophysical monitoring techniques. Our study explicitly investigates GHG variability across three successive growing seasons (2012–14) and evaluates multiple factors controlling this variability including, but not limited to, polygon geomorphology. Specifically, we consider how geomorphic, soil, vegetation and climate properties or dynamics influence CO<sub>2</sub> and CH<sub>4</sub> temporal variability through the growing seasons (intra-annual) and across years (inter-annual).

### 2.3. Datasets

Data from two transects and four representative plots were chosen for analysis in this study (Fig. 1b). These locations were chosen based on the availability of temporally-resolved data and their spatial coverage of different geomorphic features, soil and vegetation characteristics (Table 1). In particular, surface fluxes of CO<sub>2</sub> and CH<sub>4</sub> were available for 2012 and 2013 from four 160 m × 160 m plots (A–D). The sampling scheme was organized as follows: four chambers were used within each plot, covering all three polygon features (center, edge and trough) and different polygon types as represented by plots A–D, resulting in a total of forty eight (= 4 × 3 × 4) chambers. In particular, plot A lies within a low-centered polygon, plot B within a high-centered polygon and plot C within a flat-centered polygon, while plot D lies within a transitional polygon (i.e., transitional between the drained thaw-lake basins and a low-centered polygon) (Herndon et al., 2015; Lara et al., 2015). Additionally, to capture temporal variability in CO<sub>2</sub> and CH<sub>4</sub> fluxes, data were available for 2014 from two 500 m transects that traverse a broad range of polygon types and features (Hubbard et al., 2013; Wainwright et al., 2016). Twenty three chambers covering different polygon types and features were sampled across each transect, resulting in a total of forty six chambers. Note that for sampling any polygon that lacked a clear edge delineation (e.g., high-centered polygon), we placed the chamber at the upper limit of the slope between the raised center and the trough (Fig. 1c). While a possible bias in the analysis of inter-annual variability is that sampling locations varied from 2012 and 2013 to 2014, the implementation of the entropy classification scheme (described in more detail below) is such

that it considers the distribution of these flux measurements (histograms) rather than absolute values and can thereby overcome this limitation of the sampling design. Moreover, concurrent measurements of several environmental variables including soil moisture (reported as % saturation), soil temperature and information on the presence or absence of vegetation mats (moss or litter on the ground surface) were also collected along the two transects and four representative plots (Table 1). Based on these available measurements, we selected variables to represent primary controls on carbon fluxes at the site (Table 2).

Table 1. Details of the field measurements used for the entropy analysis.

<b>Location</b>	<b>Time of measurement</b>	<b>Measured variables</b>	<b>Minimum/maximum number of data points available for analysis</b>
<b>Plots A-D</b>	June 2012–Sept 2012	CO <sub>2</sub> flux, CH <sub>4</sub> flux, soil temperature (5 and 10 cm), soil moisture (5 cm depth), organic matter depth, thaw depth	152–155
<b>Plots A-D</b>	June 2013–Oct 2013	CO <sub>2</sub> flux, CH <sub>4</sub> flux, soil temperature (5, 10 and 20 cm), air temperature, soil moisture (10 and 20 cm), surface layer type, standing water depth	327–344
<b>Site 0 and site 1</b>	July 2014–Sept 2014	CO <sub>2</sub> flux, CH <sub>4</sub> flux, soil temperature (5 and 10 cm), air temperature, soil moisture (10 and 20 cm), surface layer type, standing water depth, thaw depth	108–113

Table 2. Measured variables were selected to represent primary controls that may affect carbon fluxes at the Barrow site.

<b>Primary controls on CO<sub>2</sub> and CH<sub>4</sub> fluxes</b>	<b>Selected variables for entropy-based analysis</b>
<b>Geomorphology</b>	Polygon type, polygon feature, polygon type x feature
<b>Time</b>	Intra-annual variability, Inter-annual variability
<b>Soil characteristics</b>	Soil temperature, saturation, organic matter depth, thaw depth
<b>Vegetation</b>	Surface layer type <sup>(a)</sup> , standing water depth
<b>Climatic conditions</b>	Air temperature

a. This describes whether the surface layer of the plot had standing water, a vegetation mat or both a vegetation mat and standing water.

### 2.3.1. Field measurements

CO<sub>2</sub> and CH<sub>4</sub> fluxes were measured using opaque static chambers (25 cm diameter, 15–20 cm height), seated on cylindrical PVC bases extending approximately 10 cm below the soil surface. To minimize soil disturbance, we

installed bases at the beginning of each summer and left them in place throughout the sampling season. At the top rim of each base, a 3 cm-deep, water-filled trough formed an air-tight seal with the chamber, which was vented according to Xu et al. (2006) to minimize pressure excursions due to the Venturi effect. In inundated locations, we used a floating chamber that was constructed from 25 cm diameter PVC encircled by a flat styrofoam collar. Below this collar, the bottom rim of the chamber base extended 4 cm below the water surface. As with non-floating measurements, the chamber rested in a 3 cm-deep water-filled channel in the base's top rim to create an airtight seal. For each flux measurement, we monitored CO<sub>2</sub> and CH<sub>4</sub> concentrations in the chamber every 5 s over 4–8 min with a Los Gatos Research (LGR), Inc. Portable Greenhouse Gas Analyzer, and calculated the flux of each gas as the slope of the linear portion of the concentration versus time curve. Apart from a manual evaluation, two other metrics – a slope standard error > 0.05 and the percent relative standard error (PRSE) > 5 – were used to evaluate flux measurement quality. PRSE is defined as  $100 \times (\text{slope standard error}) / (\text{slope estimate})$  as used in Sileshi (2014). Note that R<sup>2</sup> was not used here because some fluxes are close to zero, which will give a low R<sup>2</sup> even if the measurement is high-quality. Instead, this set of two metrics – the slope standard error and PRSE – avoid biasing the dataset towards either high or low flux values. Since opaque chambers limited photosynthesis during the measurement period, CO<sub>2</sub> fluxes were equivalent to ecosystem respiration.

In addition to GHG fluxes, we concurrently measured soil temperature and moisture. Volumetric soil moisture was measured using a MiniTrase TDR (Soil moisture Equipment Corp). Soil temperature was measured at multiple depths (5, 10 and 20 cm) with a hand-held thermocouple probe (Cooper-Atkins AquaTuff 352). Air temperature was also measured with a thermocouple probe and represents measurements made inside the LGR chamber. Thaw depth was measured using a tile probe and organic matter depth was analyzed using soil cores collected at the site during the same sampling campaign. Standing water depth was measured using a ruler as an average of multiple measurements of the depth of the surface layer of water. Further details on data acquisition are provided elsewhere (Torn et al., 2013; Vaughn and Torn, 2018).

### 3. Methods

#### 3.1. Shannon's informational entropy

We used the information theory metrics of Shannon's entropy to examine the temporal variability in carbon fluxes as a function of environmental factors, geomorphic features and other primary controls (Shannon, 1948a, Shannon, 1948b). Previous studies have successfully used these metrics to characterize temporal variability in climatological, geochemical, and other complex data series (e.g., Arora et al., 2016b; Balzter et al., 2015; Kawachi et al., 2001; Rajsekhar et al., 2012). In information theory, Shannon's

entropy is regarded as a measure of variability or randomness in the data, which is analogous to the lack of information about the system (Brunsell et al., 2008; Singh, 2013, Singh, 1997). Shannon's entropy ( $H$ ) of a random variable (such as time-series data) is calculated as:

$$H = - \sum_{i=1}^B P_i \log_2(P_i) \quad (1)$$

where,  $B$  is the set of measurements and  $P_i$  denotes the probability of outcome as  $i$  varies from 1 to  $B$ . Using the histogram bin width based on Scott's choice method (Scott, 1979), the discrete data interval  $i$  was determined. Eq. (1) suggests that the value of entropy varies according to the distribution of  $P_i$ 's associated with the set  $B$  chosen to represent the random variable. This implies that by increasing the number of constraints, or by specifying more information about the random variable, the range of entropy decreases. Therefore, process components that add information to the system reduce Shannon's entropy and are able to explain the variability in the data series. This concept forms the basis of our study.

Eq. (1) further indicates that there is no upper bound for entropy because if any  $P_i$  tends to 0,  $\log(.)$  will tend to infinity. Therefore, we normalize entropy as (Dwivedi, 2012):

$$H_N = \frac{\max(H)-H}{\max(H)} \times 100; \quad (2)$$

such that the normalized marginal entropy ( $H_N$ ) varies between 0 and 100. Entropy is maximum when all events are equally probable and all  $P_{i_s}$  are equal, such that.

$$\max(H) = - \sum_{i=1}^B \frac{1}{B} \log_2\left(\frac{1}{B}\right) = \log_2(B) \quad (3)$$

Thus,

$$H_N = \frac{\log_2(B)-H}{\log_2(B)} \times 100 \quad (4)$$

### 3.2. Entropy as a classification tool for GHG flux data

We employ an entropy classification scheme that exploits the property that if we add information to the system, the entropy of the system should decrease. In this study,  $\text{CO}_2$  and  $\text{CH}_4$  fluxes are the variables of interest. The addition of information to each of these random variables is done in the form of classifying flux data under different categories. For this purpose, we first

select the classifying factor and then decide the categories under which the GHG flux data can be analyzed.

The classifying factor can comprise of any of the selected variables (e.g., polygon type, soil temperature, intra-annual variability) that represent possible controls on GHG fluxes at the site (Table 2). The categories under which flux is classified will then depend on the attributes of the selected variable itself. Fig. 2 demonstrates the overall approach of the entropy classification scheme where each of the selected variables or classifying factors is partitioned into different categories. For example, polygon type is categorized as low-, flat- or high-centered polygons, while intra-annual variability is categorized as June, July, August, September or October (based on the growing season data available for each year). The classifying factor that results in a lower value of entropy explains the maximum variability in the random variable. Therefore, the environmental factor, temporal or geomorphic feature that leads to this lowest entropy value is considered to be the most important control impacting GHG fluxes at the site.

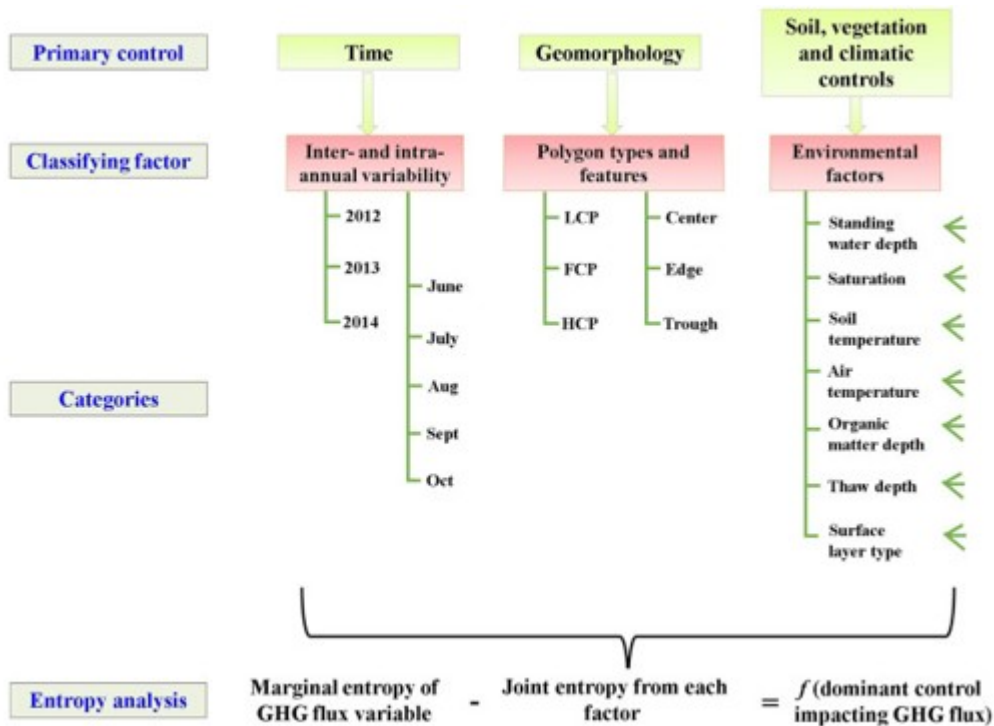


Fig. 2. An overview of the entropy classification scheme showing the primary controls, associated classifying factors and categories used for analyzing GHG fluxes in this study. As an example, the figure shows that inter-annual variability was categorized as 2012, 2013 and 2014. For variables where these categories were not obvious (e.g., thaw depth), a probability density function was used (see Fig. 3). Abbreviations: *LCP*, low centered polygon; *FCP*, flat centered polygon; *HCP*, high centered polygon.

The entropy classification scheme is implemented through the following steps:

(1) Calculate the marginal ( $H$ ) and maximum entropy ( $\max(H)$ ) of the random variable  $V$  under consideration using Eqs. (1), (3), respectively. Here,

the marginal entropy for CO<sub>2</sub> flux variable, for example, refers to the entropy computed for all CO<sub>2</sub> flux values grouped together (i.e. without any classification). However, marginal entropy values alone do not provide sufficient information about factors controlling temporal variability in CO<sub>2</sub> fluxes. We therefore proceed to the next step.

(2) Identify a set of classifying factors ( $F^1, F^2, \dots, F^s$ ) that possibly explain the variability observed in  $V$ , where the exponent  $S$  refers to the number of factors considered in the analysis. In our study, certain variables were selected to represent potential controls on GHG flux variability at the Barrow site (Table 2). Here, the choice of these factors was also based on the availability of temporally-resolved data (Table 1).

(3) Each of these classifying factors is then partitioned into different categories. For factors where these categories are not obvious, individual probability density functions (pdfs) can be used to derive representative groups. While this approach was used on multiple environmental factors, Fig. 3 shows the pdfs of only a selected subset of environmental factors to illustrate this approach.

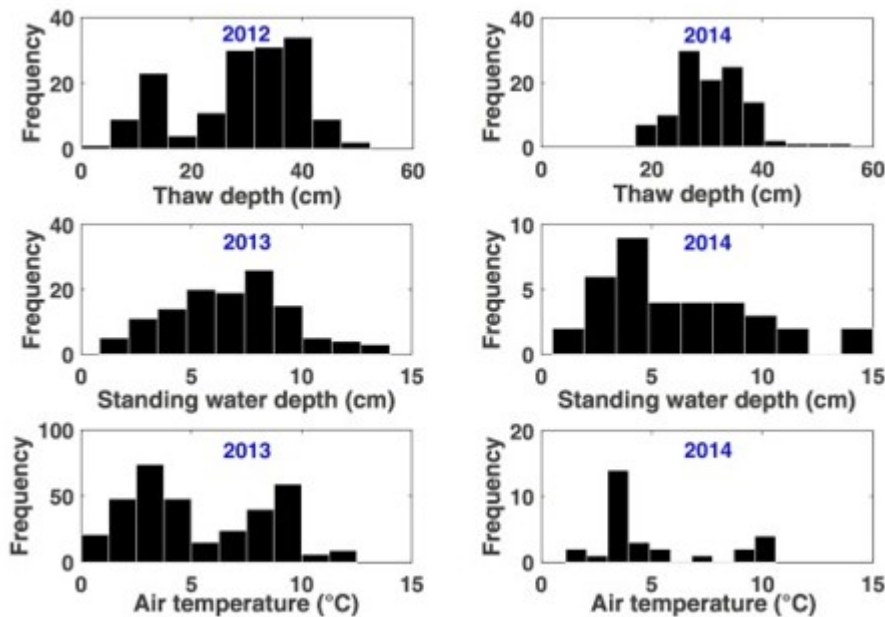


Fig. 3. Frequency distribution of selected subsets of environmental factors – thaw depth, standing water depth and air temperature – from observations for the given year (2012, 2013 or 2014). The histograms were used to divide the range of the environmental factors into different intervals or categories for the entropy-based classification scheme. Because datasets varied across years, histograms for each year were used to define these categories. Note that histograms of standing water depth do not include cases where only vegetation mats were present.

(4) Calculate the joint probability  $H(V, F^1, F^2, \dots, F^s)$  and the conditional probability  $H(V|F^c)$  of the random variable when the data is classified according to different categories for each factor  $F^c$  ( $c \in 1:s$ ). Details of these probability calculations are provided in Supporting Information (S1).

(5) The quantity of information shared between the two variables (in this case, GHG flux and each classifying factor) is then obtained by calculating  $H(V) - H(V|F^c)$ , which is also known as trans-information ( $T$ ). For comparing entropy values across different factors, we used a normalized measure of trans-information ( $T_N$ ).

(6) Here the objective is to maximize  $T_N$  (or minimize entropy) to identify factors that explained the most variability in data.

To appreciate the value of trans-information, the equation reported in step (5) can be interpreted as follows: here,  $H(V)$  represents the uncertainty (or information) about CO<sub>2</sub> or CH<sub>4</sub> fluxes before observing any classifying factor ( $F$ ) and the conditional entropy  $H(V|F^c)$  represents the uncertainty in the fluxes after accounting for the factor, the difference between  $H(V)$  and  $H(V|F^c)$  thus represents the uncertainty that is reduced by observing the factor. Therefore, trans-information represents the amount of variability in GHG fluxes that is reduced when  $F$  is known. The strength of this classification scheme lies in its ability to identify primary controls that cause significant variability in GHG fluxes across years. The implementation of the classification scheme is such that it can be used on data sets of different lengths and can analyze different spatial settings (as is this case with our sampling campaign) (Dwivedi and Mohanty, 2016; Gaur and Mohanty, 2013). To further account for the effect of different numbers of data points and comparing entropy values across years, we calculated the difference between the normalized trans-information ( $T_N$ ) and the normalized entropy of the flux variable for that year ( $H_{N, year}$ ):

$$D = T_N(V, F^c) - H_{N, year} \quad (5)$$

such that  $D$  describes the variability in GHG flux due to the classifying factor for that year. The greater the difference (or the greater the ' $D$  value'), the more informative is that factor for explaining variability in the fluxes. In particular,  $D$  values greater than 0 indicate significant variability in GHG fluxes due to that factor, while values less than 0 indicate insignificant variability. Apart from GHG fluxes, we also demonstrate the applicability of the entropy classification scheme to other variables of interest, in particular soil temperature at 5 cm depth (see Section 4.4).

### 3.3. Kruskal-Wallis significance testing

Statistical significance was evaluated using the two-sided, two-sample Kruskal-Wallis test (also termed the Mann-Whitney-Wilcoxon test) (Kruskal and Wallis, 1952; Mann and Whitney, 1947). The Kruskal-Wallis significance test is the non-parameteric equivalent of the analysis of variance test and provides a more elegant solution when data are suspected to be from a non-normal distribution. Here, the Kruskal-Wallis significance test was used to determine if a particular category resulted in a significant separation of the median GHG flux values by testing the null hypothesis that there is no

difference in the median GHG flux values across categories of a particular classifying factor, against the alternative that they do not have equal medians. The Kruskal-Wallis test results were considered significant at a *p*value equal to or less than 0.05.

## 4. Results

### 4.1. Site trends in CO<sub>2</sub> and CH<sub>4</sub> fluxes

Fig. 4 shows the mean fluxes of CO<sub>2</sub> and CH<sub>4</sub> across polygon types for 2012, 2013 and 2014 growing season. While mean CO<sub>2</sub> fluxes show minor differences across polygon types (small range of variation), mean CH<sub>4</sub> fluxes show clear patterns with highest fluxes being associated with LCPs. The temporal patterns for both CO<sub>2</sub> and CH<sub>4</sub> fluxes show more variability. In particular, GHG fluxes show an increase from 2012 to 2013 and then a decrease from 2013 to 2014. One exception to this trend is that CO<sub>2</sub> fluxes show a consistently increasing pattern from 2012 to 2014 for HCPs. In fact, the highest ecosystem respiration in 2014 is associated with HCPs. To investigate possible controls of such variations, we describe multi-year trends in measured soil moisture and soil temperature values at the site (Fig. 5). Fig. 5 suggests that 2013 was a relatively dry growing season as compared to 2012 or 2014, whereas soil temperature values indicate that 2014 was a relatively cold year. In a simplistic view, the characteristics of these years suggest that flat-centered polygons may become important sources of CO<sub>2</sub> during warm and dry years as opposed to high-centered polygons which contribute to CO<sub>2</sub> efflux during cold and wet years. However, it is not yet clear if soil moisture or soil temperature characteristics alone, or in combination with other environmental factors control GHG flux variations under different spatio-temporal settings.

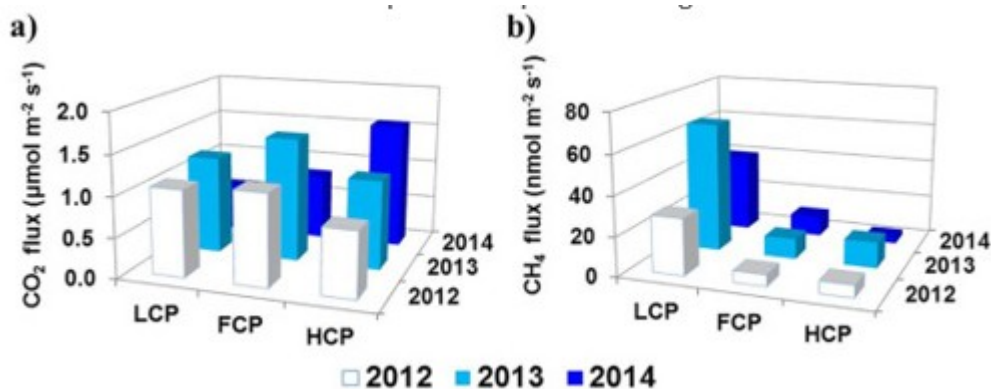


Fig. 4. Spatial and temporal variability in measured arithmetic mean a) CO<sub>2</sub> and b) CH<sub>4</sub> fluxes at the site during the growing season for three successive years. Abbreviations: *LCP*, low centered polygon; *FCP*, flat centered polygon; *HCP*, high centered polygon.



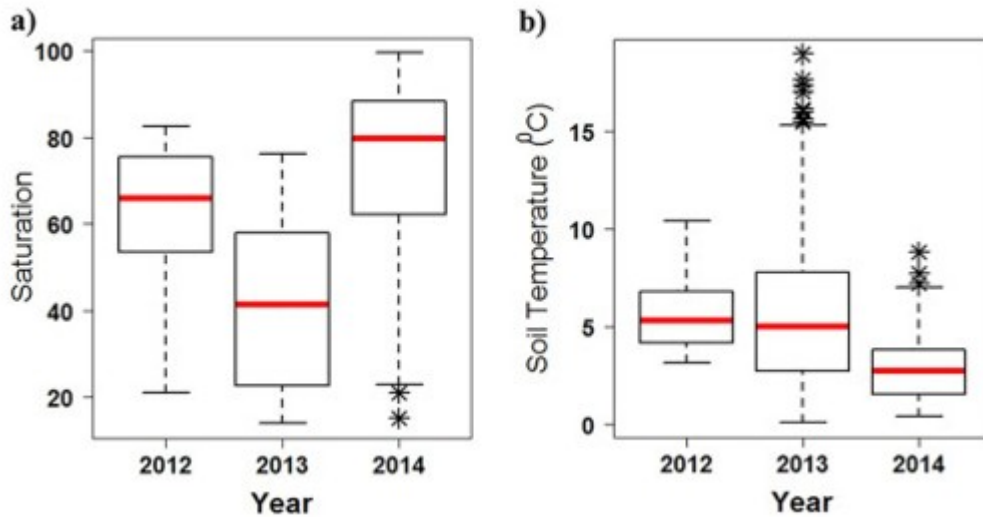


Fig. 5. Box plots of measured a) saturation and b) soil temperature values collected during 2012, 2013 and 2014 growing season. The top and bottom of the box represent the 25th and 75th percentiles, respectively, the central red line is the median, the whisker-lines indicate the 99% interval, and stars indicate outliers.

#### 4.2. Evaluating temporal controls of CO<sub>2</sub> fluxes

To classify CO<sub>2</sub> fluxes according to the selected geomorphic feature or environmental factors, we calculated the trans-formation and the corresponding difference ( $D$ ) with the marginal entropy value of CO<sub>2</sub> for that year as outlined in the classification scheme above. Fig. 6 shows the plot of this difference  $D$  when CO<sub>2</sub> fluxes are classified on the basis of polygon types and features. As is evident from the figure, both LCP edges and HCP centers show  $D$  values greater than 0 for 2012. Fig. 6 further shows that LCP edges as well as HCP edges and troughs have  $D$  values greater than 0 for 2013, while only LCP edges show this pattern for 2014. Therefore, only LCP edges consistently show  $D$  values greater than 0 for all years. This suggests that significant variability is associated with CO<sub>2</sub> fluxes in LCP edges across years. However, only higher topographic positions (i.e., LCP edges and HCP centers) show  $D$  values greater than 0 across years as compared to lower topographic positions (i.e., LCP centers and troughs). One reason for this variability could be that higher topographic positions typically have lower soil moisture content (such as LCP edges) or have well-drained oxic soils (such as HCP centers) in comparison to lower elevation regions (Fig. S1, Supplementary Information) (Hubbard et al., 2013; Wainwright et al., 2015). Changes in oxygen availability and soil moisture content in higher topographic positions can cause significant variations in ecosystem respiration. Fig. 5, Fig. 7 confirm that the overall soil moisture range shows considerable variability across years and especially within the LCP edges. Further note that results associated with plot D, which lies within a transitional region and is represented by cyan filled symbol, demonstrated atypical response for LCP edges across all years, possibly due to its waterlogged condition and different hydrological characteristics than typical LCPs (Fig. 6).

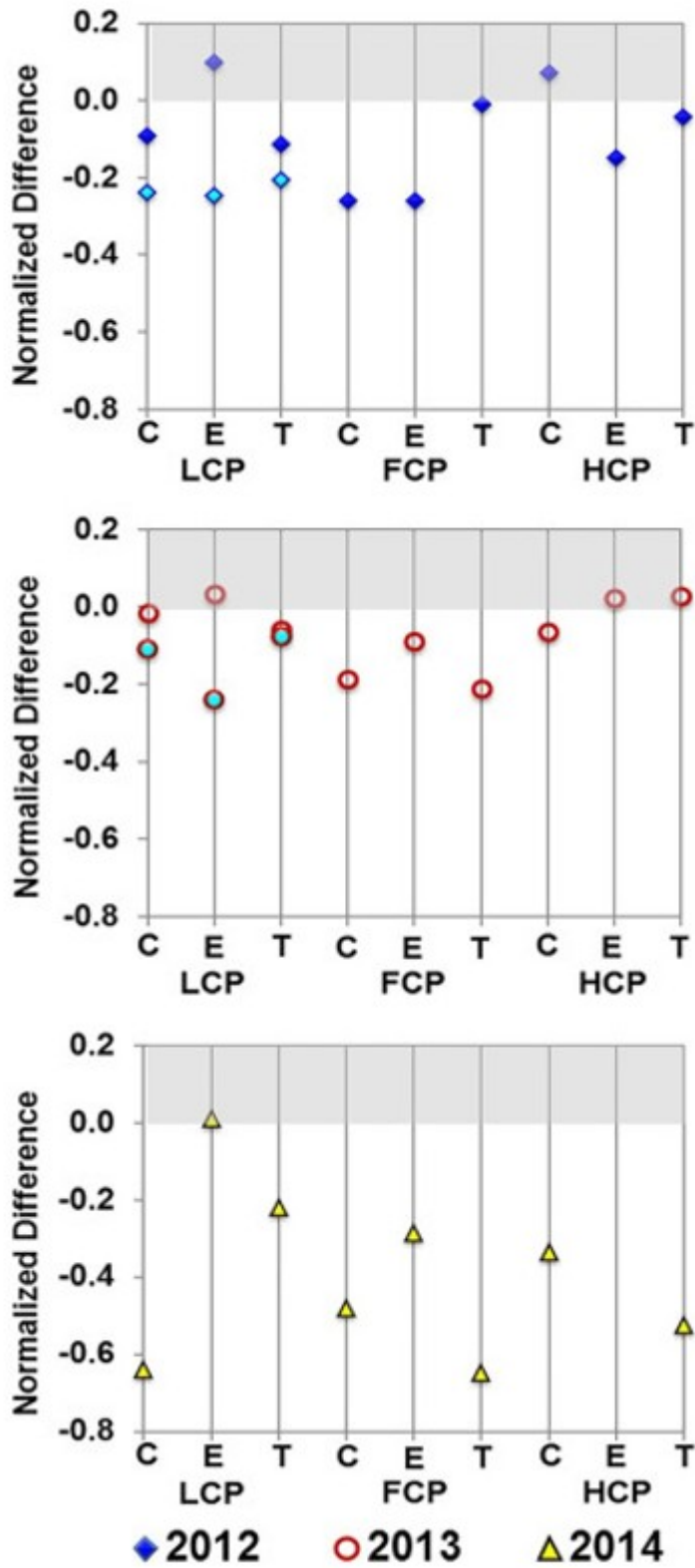


Fig. 6. Normalized difference ( $D$ ) values for CO<sub>2</sub> flux across polygon types and features. Normalized  $D$  values greater than 0 at a particular location indicate significant variability in CO<sub>2</sub> fluxes at that location. Cyan filled symbols are used to separate plot D results from plot A because of their distinct

hydrological characteristics. Abbreviations: *LCP*, low centered polygon; *FCP*, flat centered polygon; *HCP*, high centered polygon; *C*, center; *E*, edge; *T*, trough.

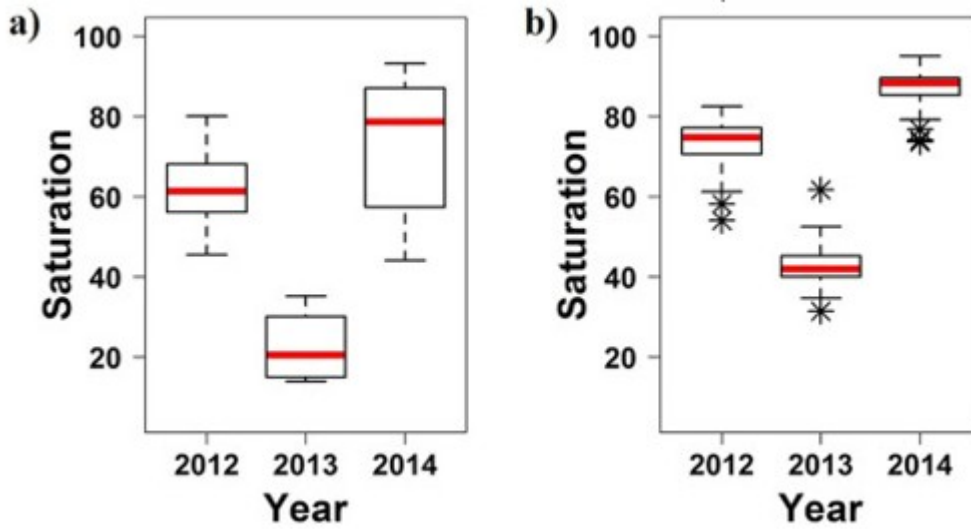


Fig. 7. Box plot of saturation within a) LCP edges and b) LCP centers collected during 2012, 2013 and 2014. The top and bottom of the box represent the 25th and 75th percentiles, respectively, the central red line is the median, the whisker-lines indicate the 99% interval, and stars indicate outliers.

To further characterize temporal variability at the site, Fig. 8 shows the plot of the normalized difference  $D$  when  $\text{CO}_2$  fluxes are classified according to polygon types and intra-annual variability. As expected, higher  $D$  values and consequently higher variability is associated with LCPs for both 2012 and 2013 (Fig. 8a). In contrast, all  $D$  values for 2014 are below 0. As suggested in the previous section and shown in Table 3,  $\text{CO}_2$  flux patterns within 2014 show consistently different trends (Kruskal-Wallis test,  $p < 0.0001$ ) as compared to 2012 or 2013. Fig. 8b demonstrates that early growing season months (June 2012 and July 2013) have  $D$  values greater than 0, as well as late growing season months (September 2012 and October 2013) have  $D$  values above 0. 2014 again shows a different pattern for  $\text{CO}_2$  flux variability wherein the peak growing season (August) has  $D$  values greater than 0. For 2012 and 2013, these results indicate that the early and late growing season periods cause significant variability in  $\text{CO}_2$  fluxes. Fig. 9a confirms that although the highest ecosystem respiration across years is associated with August, the lower  $\text{CO}_2$  flux values show considerable variability across early and late growing season months. Moreover, the Kruskal-Wallis test indicates a substantial separation ( $p < 0.0001$ ) of mean  $\text{CO}_2$  fluxes across growing season months, but demonstrates insignificant separation ( $p > 0.05$ ) of  $\text{CO}_2$  fluxes as a function of other vegetation-related parameters (e.g., the presence or absence of vegetation, standing water depth) (Table 3). This implies that early and late season dynamics or lengthening of the growing season may be responsible for significant variability in  $\text{CO}_2$  fluxes at the site. Other site-specific and regional investigations have reported progressively earlier spring snowmelt date and later onset of autumn snow accumulation (Cox et al., 2017; Sharratt, 1992; Tucker et al., 2001; Zona et

al., 2016). In their study, Oechel et al. (1995) described significant differences in ecosystem respiration and net CO<sub>2</sub> fluxes at Barrow during the late growing seasons of 1991 and 1992 as compared to measurements made in the International Biological Program in 1971 over a comparable period, and attributed these changes to increased air temperatures and resulting decrease in soil moisture content. This significant variability in CO<sub>2</sub> fluxes in 2012 and 2013 may therefore be related to recent temperature trends and increasing length of the growing season, but additional work is needed to substantiate these associations. Further note that 2014 was a colder year in comparison to 2012 and 2013 (Fig. 5b) and reported CO<sub>2</sub> flux patterns consistently different from previous years at the site.

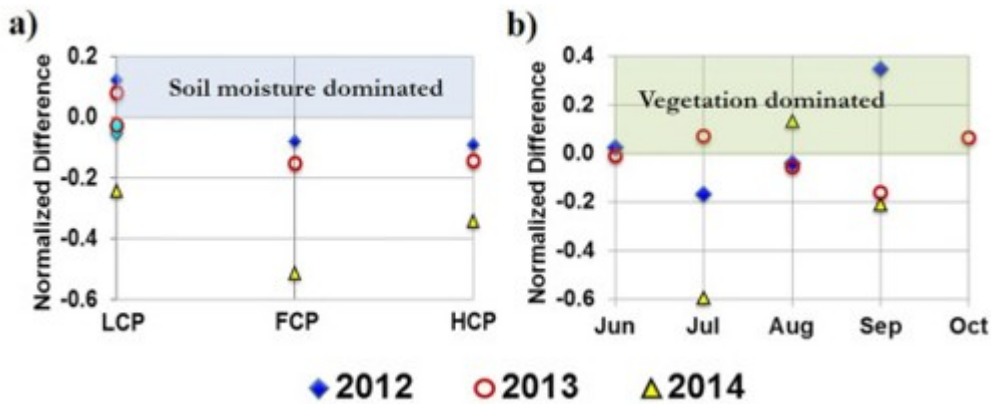


Fig. 8. Normalized difference ( $D$ ) values for CO<sub>2</sub> flux across a) polygon types and b) growing season months. Normalized  $D$  values greater than 0 indicate significant variability in CO<sub>2</sub> fluxes at that location or for that month. Cyan filled symbols are used to separate plot D results from plot A because of their distinct hydrological characteristics. Abbreviations: *LCP*, low centered polygon; *FCP*, flat centered polygon; *HCP*, high centered polygon.

Table 3.  $D$  values for CO<sub>2</sub> flux computed on the basis of different classifying factors<sup>a</sup>.

Primary Control	Classifying factor	Categories	<i>D</i> values for CO <sub>2</sub> flux			
			2012	2013	2014	Repeating pattern
Geomorphology	Polygon type	LCP, HCP, FCP	12.66 <sup>b</sup> (LCP)	8.47 (LCP)		
	Polygon feature	Center, Edge, Trough	11.19 (Edge)			
	Polygon type × feature	(LCP, HCP, FCP) × (Center, Edge, Trough)	10.20 <sup>b</sup> (LCP × Edge; HCP × Center)	3.62 <sup>b</sup> (LCP × Edge; HCP × Edge; HCP × Trough)	0.10 <sup>b</sup> (LCP × Edge)	LCP × Edge
Climate	Air temperature	<3, 3 to 6, 6 to 9, 9 to 12 °C		15 <sup>b*</sup> (<3)	13.43 <sup>b*</sup> (2 and 3.5)	Air temperature between 2 and 3
Soil	Soil temperature	<3, 3 to 5, 5 to 7, 7 to 10, >10 °C	11.18 <sup>b*</sup> (3 to 5)	9.42 <sup>b</sup> (5 to 10 and 15 to 20)	15.53 <sup>b</sup> (< 3)	Low soil temperature (<10)
	Organic matter depth	<10, 10 to 15, 15 to 20 cm	7.65 (<10)			
	Thaw depth	<15, 15 to 30, 30 to 45, 45 to 60 cm	3.66 (45 to 60)			
	Saturation	0 to 20, 20 to 40, 40 to 60, 60 to 80%				
Vegetation	Surface layer type	Water, vegetation, water and vegetation				
	Standing water depth	<5, 5 to 10, 10 to 15 cm		0.89 (10 to 15)		
Time	Intra-annual variability	June, July, Aug, Sept, Oct	35.07 <sup>b*</sup> (Jun, Sept)	7.28 <sup>b*</sup> (July, Oct)	13.43 <sup>b*</sup> (Aug)	Early and late season periods
	Inter-annual variability	2012, 2013, 2014			12.99 <sup>b*</sup> (2014)	

<sup>a</sup>Shaded cells show where data are not available.

<sup>b</sup>A significant separation of means with  $p < 0.05$ .

<sup>\*</sup> $p < 0.0001$ .

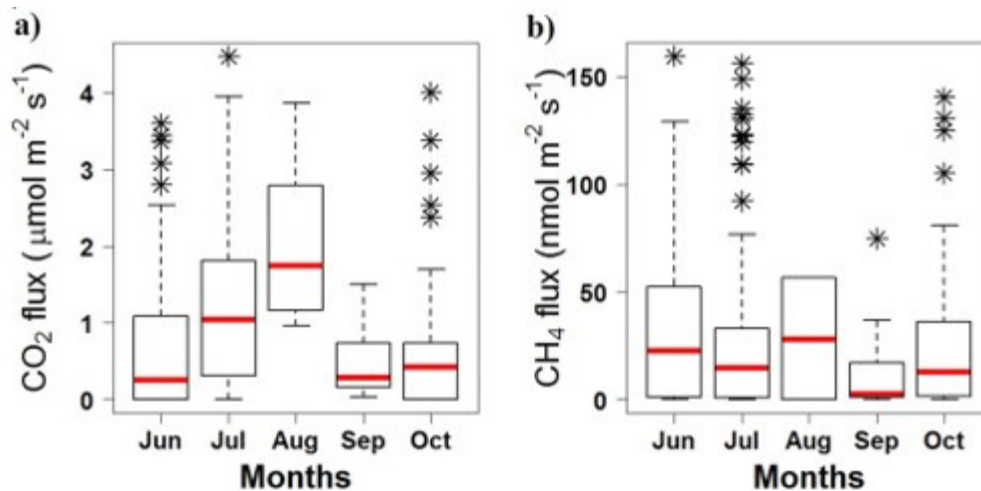


Fig. 9. Box plots of a) CO<sub>2</sub> and b) CH<sub>4</sub> flux values for the 2013 growing season. The top and bottom of the box represent the 25th and 75th percentiles, respectively, the central red line is the median, the whisker-lines indicate the 99% interval, and stars indicate outliers.

A summary of the entropy results identifying the governing controls on CO<sub>2</sub> flux variability is provided in Table 3. The table shows the classifying factors used (column 2), the categories under which the classification was performed (column 3), and the specific category that resulted in a difference between transfer entropy and CO<sub>2</sub> entropy to be greater than 0 (columns 4 to 6). The last column indicates if a particular category resulted in *D* values that were consistently greater than 0 across all years. This column is important to understand where the variability in the data was constantly higher and can help with developing a strategic plan for sampling in multi-year studies or identifying controls that should be included in modeling GHG fluxes. For ease of interpretation of the table, we present an example wherein soil temperature is used as a classifying factor and is subdivided into several categories. Results from Table 3 suggest that low soil temperature (<10 °C) is a recurring factor causing variability in CO<sub>2</sub> trends across years at a significance level of 0.05.

Overall, CO<sub>2</sub> fluxes at the Barrow site show considerable temporal variability at the site. This variability is attributed to factors that impact soil (e.g., temperature, moisture conditions) and/or vegetation dynamics (e.g., growing season length). Significant variability in ecosystem respiration was also associated with higher topographic positions. Moreover, CO<sub>2</sub> flux patterns in 2014 were found to be consistently different than those observed in 2012 or 2013. Unlike 2014, 2013 which had characteristically low soil moisture content did not show significantly different patterns for CO<sub>2</sub> fluxes when compared to 2012 (e.g., using inter-annual variability as a classifying factor in Table 3). This clearly indicates that soil moisture characteristics alone were not significant controls ( $p > 0.05$ ) on CO<sub>2</sub> flux variability at the site, but may act in tandem with the unique property suites of higher topographic positions (such as LCP edges) or higher air temperatures (e.g., Oechel et al., 1995) to impact CO<sub>2</sub> efflux from the site.

#### 4.3. Evaluating temporal controls of CH<sub>4</sub> fluxes

To investigate the temporal patterns in CH<sub>4</sub> fluxes at the site, we followed the same procedure of classifying flux data according to different factors (Table 4). Table 4 indicates that HCP centers show consistently high variability in CH<sub>4</sub> fluxes across years. Variability is also observed in FCP centers and edges for both 2012 and 2014 but not for 2013 (Fig. 10a). These polygon types and positions are associated with different CH<sub>4</sub> production pathways (via CO<sub>2</sub> reduction) as compared to LCPs where acetate cleavage is the main production mechanism (Vaughn et al., 2016). Consistent with the previous findings, we therefore attribute this variability in CH<sub>4</sub> fluxes to topographic position or geomorphic controls. The Kruskal-Wallis test also substantiates these findings demonstrating a significant separation ( $p < 0.0001$ ) of mean CH<sub>4</sub> fluxes across topographic positions.

Table 4.  $D$  values for  $\text{CH}_4$  flux computed on the basis of different classifying factors<sup>a</sup>.

Primary Control	Classifying factor	Categories	$D$ values for $\text{CH}_4$ flux			
			2012	2013	2014	Repeating pattern
Geomorphology	Polygon type	LCP, HCP, FCP			2.70 <sup>b*</sup> (HCP, FCP)	
	Polygon feature	Center, Edge, Trough				
	Polygon type × feature	(LCP, HCP, FCP) × (Center, Edge, Trough)	45.15 <sup>b*</sup> (HCP × Center)	14.37 <sup>b*</sup> (HCP × Center)	40.22 <sup>b*</sup> (HCP × Center)	HCP × Center
Climate	Air temperature	<3, 3 to 6, 6 to 9, 9 to 12 °C				
Soil	Soil temperature	<3, 3 to 5, 5 to 7, 7 to 10, >10 °C	9.18 (7 to 10)		10.95 <sup>b</sup> ( < 3)	
	Organic matter depth	<10, 10 to 15, 15 to 20 cm				
	Thaw depth	<15, 15 to 30, 30 to 45, 45 to 60 cm	27.62 (30 to 45 and 45 to 60)		28.30 <sup>b</sup> (0 to 30 and 45 to 60)	High thaw depth (45 to 60)
	Saturation	0 to 20, 20 to 40, 40 to 60, 60 to 80%	45.15 <sup>b*</sup> (0 to 40)	6.70 <sup>b*</sup> (0 to 40)	19.42 <sup>b*</sup> (0 to 40)	Low soil moisture (0 to 40%)
Vegetation	Surface layer type	Water, vegetation, water and vegetation		0.64 <sup>b*</sup> (Vegetation)	0.16 <sup>b*</sup> (Vegetation)	Vegetation
	Standing water depth	<5, 5 to 10, 10 to 15 cm				
Time	Intra-annual variability	June, July, Aug, Sept, Oct	6.45 <sup>b*</sup> (Aug)			
	Inter-annual variability	2012, 2013, 2014				

<sup>a</sup>Shaded cells show where data are not available.

<sup>b</sup>A significant separation of means with  $p < 0.05$ .

\* $p < 0.0001$ .

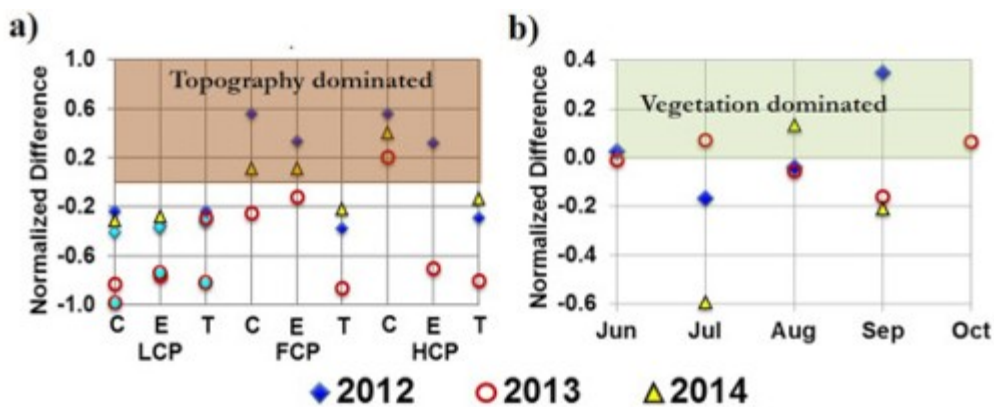


Fig. 10. Normalized difference ( $D$ ) values for  $\text{CH}_4$  flux across a) polygon types and features as well as b) growing season months. Normalized  $D$  values greater than 0 indicate significant variability in  $\text{CH}_4$  fluxes at that location or for that month. Cyan filled symbols are used to separate plot  $D$  results from plot A because of their distinct hydrological characteristics. Abbreviations: *LCP*, low centered polygon; *FCP*, flat centered polygon; *HCP*, high centered polygon; *C*, center; *E*, edge; *T*, trough.

Another factor associated with high variability ( $p < 0.0001$ ) in CH<sub>4</sub> fluxes across years is the presence or absence of vegetation (Table 4). Fig. S2 further expands on these results to demonstrate the impact of vegetation type and ponded conditions on CH<sub>4</sub> emissions, however a complete analysis of ebullitive fluxes versus fluxes from submerged vegetation or assessing the impact of plant height is beyond the scope of this study. However, growing season (intra-annual) variability does not seem to be a recurring factor causing variability in CH<sub>4</sub> profiles at the site (Table 4). Nevertheless, Fig. 9b demonstrates the variability in CH<sub>4</sub> fluxes across growing season months for the 2013 sampling campaign. Similar to Fig. 9b, but comprehensively including other years in the analysis, Fig. 10b demonstrates that vegetation changes within the growing season result in  $D$  values greater than 0 and thereby significant variability in CH<sub>4</sub> fluxes, albeit at different times. The reasons for this discrepancy will be described below.

Table 4 further suggests that regions with greater thaw depths (45 to 60 cm) and lower soil moisture (<40% saturation) show significant variability in CH<sub>4</sub> fluxes across years. Note that thaw depths are significantly linked to topographic position and consequently with soil moisture and vegetation cover. In particular, low topographic positions (such as LCP centers) have greater thaw depths, higher water table and are typically vegetated with vascular plants (Kumar et al., 2016; Walker et al., 2008). In contrast, higher topographic positions (such as HCP centers) are associated with shallower thaw depths, lower saturation and less vegetation cover. Thus, when thaw depth and vegetation cover are considered to be classifying factors (Table 4), variability in CH<sub>4</sub> fluxes can be attributed to low topographic positions (such as LCP centers) based on its association with greater thaw depths and vegetative cover. In contrast, when polygon type and feature as well as saturation are considered as classifying factors, variability in CH<sub>4</sub> fluxes can be attributed to high topographic positions (such as HCP centers). The Kruskal-Wallis test also shows substantial differences ( $p < 0.0001$ ) in mean CH<sub>4</sub> fluxes when classified according to most of these factors (e.g., saturation, vegetation cover). Taken together, these results attribute variability to both high and low topographic positions, and this is because the temporal relationships between vegetation and primary controls (e.g., soil moisture, thaw depth) change during the growing season and in distinct ways for the different topographic positions. Earlier in the growing season, the lower topographic positions have greater thaw depth and higher soil moisture, which can result in an earlier activation of the ecosystem for CH<sub>4</sub> fluxes (Zona et al., 2009). In contrast, the ground is still largely frozen in the higher topographic positions and the water availability to the plants is lower resulting in lower CH<sub>4</sub> fluxes from these regions. However, later in the season, CH<sub>4</sub> emissions from higher topographic positions can increase as thawing progresses. These results also match with findings from Dafflon et al. (2017) that demonstrated the changing relationship between vegetation and soil moisture as well as between vegetation and thaw layer thickness



during the growing season using above- and below-ground geophysical monitoring approaches. Fig. 10b further confirms these changing dominant controls with  $D$  values becoming greater than 0 at different times within the growing season. The variability in  $\text{CH}_4$  fluxes at the Barrow site can therefore be attributed to both direct (e.g., plant productivity) and indirect impacts (e.g., vegetation-thaw relationship) of vegetation changes during the growing season.

#### 4.4. Using entropy for monitoring and predicting GHG fluxes

Studies on quantifying carbon fluxes typically suffer from insufficient observations across relevant spatial and temporal scales and a lack of knowledge about dominant environmental variables that can consistently represent this variability across scales. The entropy classification scheme can bring a range of benefits to data acquisition and model development, particularly with identifying a set of primary controls that can describe variability in GHG fluxes. These primary controls can then be used as deterministic variables for developing relationships or designing upscaling techniques for estimating footprint- or global-scale GHG fluxes from field-scale measurements. Furthermore, as the need for long-term data acquisition becomes more urgent in the face of changing climate, the entropy classification scheme can be applied to identify uncertainties (or randomness) in existing observations and design an efficient data acquisition strategy for subsequent years. Here, we present an example of applying the entropy classification scheme to identify a set of factors that cause variability in environmental data. Specifically, we consider the case of soil temperature at the Barrow site which has been associated with variability in  $\text{CO}_2$  trends while the nature of its relationship with  $\text{CH}_4$  fluxes is more uncertain (Table 3, Table 4). Although this example is focused on designing sampling strategies geared towards GHG flux determination and future predictions, the following approach is generic enough for identifying dominant controls that can describe variability in other variables of interest.

Table 5 presents the results of analyzing soil temperature using the entropy classification scheme. In this case, the ultimate aim of the entropy analysis is to identify potential spatial locations or time periods where data collection can be prioritized, which is crucial for subsequent flux analysis. Table 5 indicates that HCP centers show consistently high variability ( $p < 0.05$ ) in soil temperature data across years. In fact, the highest  $D$  values in 2012 are associated with LCP edges. Therefore, significant variability in soil temperature data at shallow depths is associated with higher topographic positions. Previous studies have indicated that patterns of albedo, thermal conductivity, thicker snow depth and greater vegetative cover act together to cause greater heat trapping in the lower topographic positions as compared to higher topographic positions (i.e., HCP centers and LCP edges) (Gamon et al., 2012; Juszak et al., 2016). The insulating effects of the thicker snow cover and vegetative layer in low elevation regions and the lack thereof in high elevation regions can create soil microclimates that can result

in significant spatial heterogeneity in soil temperature profiles across polygon types and features.

Table 5. *D* values for soil temperature computed on the basis of different classifying factors<sup>a</sup>.

Primary Control	Classifying factor	Categories	Higher <i>D</i> values indicate factors that explain more of the soil temperature variability. Value in parenthesis identifies the category that resulted in these higher <i>D</i> values.			
			2012	2013	2014	Repeating pattern
Geomorphology	Polygon type	LCP, HCP, FCP	7.78 (LCP, FCP)	11.10 <sup>b</sup> (HCP, FCP)	5.55 (LCP, HCP)	
	Polygon feature	Center, Edge, Trough	1.21 <sup>b</sup> (Center)	0.02 <sup>b*</sup> (Center)	7.52 (Edge, Trough)	
	Polygon type × feature	(LCP, HCP, FCP) × (Center, Edge, Trough)	25.88 <sup>b</sup> (HCP × Center; FCP × Center; LCP × Edge)	3.50 <sup>b*</sup> (HCP × Center; FCP × Center)	24.24 <sup>b</sup> (FCP × Edge; HCP × Center)	HCP × Center
Climate	Air temperature	<3, 3 to 6, 6 to 9, 9 to 12 °C		1.82 <sup>b*</sup> (<3, 3 to 6)	16.27 <sup>b*</sup> (<3, 6 to 9)	<3
Soil	Organic matter depth	<10, 10 to 15, 15 to 20 cm	4.15 <sup>b</sup> (below 10)			
	Thaw depth	<15, 15 to 30, 30 to 45, 45 to 60 cm	17.00 <sup>b*</sup> (<15 and 45 to 60)		34.76 (30 to 45 and 45 to 60)	45 to 60
	Saturation	0 to 20, 20 to 40, 40 to 60, 60 to 80%	12.28 (0 to 40)	7.70 <sup>b</sup> (0 to 40 and 60 to 80)	15.71 <sup>b</sup> (0 to 40 and 80 to 100)	Low soil moisture (0 to 40%)
Vegetation	Surface layer type	Water, vegetation, water and vegetation		30.02 <sup>b*</sup> (Vegetation)	5.00 <sup>b</sup> (Vegetation)	Vegetation
	Standing water depth	<5, 5 to 10, 10 to 15 cm		19.90 <sup>b</sup> (<5, 5 to 10 and 10 to 15)	17.82 (<4, 4 to 8 and 8 to 15)	<15
	Intra-annual variability	June, July, Aug, Sept, Oct	14.28 <sup>b*</sup> (Sept)	36.57 <sup>b*</sup> (June, Sept)	7.33 <sup>b*</sup> (Sept)	September
Time	Inter-annual variability	2012, 2013, 2014				
	Depth	5, 10 and 20 cm	3.5 <sup>b*</sup> (5 cm)	11.5 <sup>b*</sup> (5 cm)	21.36 <sup>b*</sup> (5 cm)	5 cm

<sup>a</sup>Shaded cells show where data are not available.

<sup>b</sup>A significant separation of means with  $p < 0.05$ .

\* $p < 0.0001$ .

Entropy results further indicate that variability is also observed in vegetated and high thaw depth regions as well as in low soil moisture conditions (Table 5). Therefore, like CH<sub>4</sub> flux, variability in soil temperature at 5 cm depth can be associated with both low and high topographic positions. This further suggests that the relationships between soil temperature and primary controls on soil microclimate (e.g., vegetation, thaw depth, air temperature) change during the growing season and in distinct ways for the different topographic positions. The Kruskal-Wallis test also shows significant differences ( $p < 0.05$ ) in mean soil temperature when classified according to most of these factors. Other factors that cause substantial variability ( $p < 0.0001$ ) in soil temperature data are low air temperature and inter-annual variability. Note that these factors also caused variability in CO<sub>2</sub> fluxes (Table 3). In addition to these classifying factors, we further investigated the variability or randomness in soil temperature data collected

at different depths. As expected, the entropy analysis indicates that soil temperature data show significant variability ( $p < 0.0001$ ) at shallow depth (5 cm) as compared to measurements made at relatively deeper depths (10 or 20 cm).

Overall, significant variability in soil temperature data at the Barrow site is associated with geomorphic features where vegetation, snow cover and other primary controls contribute to local soil microclimatic conditions, which can vary both spatially and temporally. In terms of designing an efficient data acquisition strategy, the entropy analysis calls for improved sampling in locations that are characteristically difficult to sample, such as LCP edges or ponded locations. Results further indicate that significant variability is associated with shallow soil temperature measurements (5 cm), which is also expected. The analysis thus suggests that the choice of soil depth at which soil temperature data (e.g., 10 cm depth) are used will impact predictions of GHG fluxes (e.g., Sachs et al., 2008; Subke and Bahn, 2010). Table 5 further indicates that considerable variability ( $p < 0.0001$ ) in soil temperature is related to the month of September. This could be related to vegetation senescence or the initial freeze-back period, which can have an impact on soil microclimatic conditions.

## 5. Summary and conclusions

We used an entropy-based approach to identify dominant environmental factors associated with significant variability in GHG fluxes in Arctic tundra environments, where climate change appears to be rapidly impacting ecosystem processes. In particular, we classified growing season flux data from 2012 to 2014 using a variety of environmental factors and topographic positions across the Barrow site. CO<sub>2</sub> fluxes in 2014 were found to be significantly different than the other two sampling seasons. Entropy analysis indicated that temporal variability in CO<sub>2</sub> flux is governed by soil temperature variability, vegetation changes during the early and late growing season, and changes in soil moisture at higher topographic locations. The variability in CH<sub>4</sub> flux at the site is primarily associated with vegetation changes during the growing season and temporal shifts in relationships between vegetation and environmental factors such as thaw depth. Polygon types and features were found to be important controls on the temporal variability of both CO<sub>2</sub> and CH<sub>4</sub> fluxes at the site.

There are two interesting conclusions from the entropy analysis on GHG fluxes observed here. First, different environmental factors explained variability in GHG fluxes under different spatio-temporal settings. For example, soil moisture explained the majority of the variability in CO<sub>2</sub> fluxes across geomorphic features, while soil temperature and early and late growing season dynamics explained variability across years. Second, the mechanisms with which the environmental factors shape the spatial and temporal variability in GHG fluxes may become important to the total GHG flux budget considering the changing climate. For example, results suggest

that recent temperature trends and increasing length of the growing season may act to change CO<sub>2</sub> fluxes observed at the site. In particular, flat-centered polygons may become important sources of CO<sub>2</sub> during warm and dry years, while high-centered polygons may become important during cold and wet years. Predictive modeling of the site also concurs that higher topographic positions may become net C sources in the future (Grant et al., 2017). In contrast, the relationship between soil temperature and CH<sub>4</sub> flux shows a dynamic nature across years and appears to be sensitive to soil microclimatic conditions that show considerable spatial and temporal heterogeneity. This suggests that the strength and nature of the relationship between certain environmental factors and GHG fluxes can vary temporally and spatially, and/or the sensitivity of these factors can be masked by other variables. Depending on how the harsh Arctic environment impacts these environmental controls, the observation of these controls in subsequent sampling seasons and the mechanisms with which they impact GHG fluxes will provide an important link between climate change and GHG emissions.

Considering that the identification of primary controls on GHG flux variability is an important aspect of developing upscaling techniques or reducing model uncertainty, concepts from the entropy classification scheme can be used for this purpose. As an example, this study demonstrates the use of entropy classification scheme in developing a sampling strategy for subsequent years, by which the GHG flux predictions can be inferred with certainty, while minimizing the amount of data that must be gathered. In particular, we recommend high resolution sampling of soil temperature at HCP centers and during the month of September. This month marks the time when freeze-back period begins, which has important implications for vegetation senescence and changes in soil microclimatic conditions. Further note that our three year dataset had enough natural variability in dominant environment factors such as soil moisture and temperature to be useful to inform future sampling efforts. For other studies, the ideal number of years which can be used to inform sampling efforts may vary depending on the range of environmental conditions over which important interactions occur, collecting observations at the relevant spatial and temporal scales at which these interactions occur and sampling the specific environment of interest.

### Acknowledgments

This material is based upon work supported as part of the Next-Generation Ecosystem Experiments (NGEE-Arctic) at Lawrence Berkeley National Laboratory funded by the U.S. Department of Energy, Office of Science, Office of Biological and Environmental Research under Award Number DE-AC02-05CH11231.

### References

Arora and Mohanty, 2017

B. Arora, B.P. Mohanty **Influence of spatial heterogeneity and hydrological perturbations on redox dynamics: a column study**

Procedia Earth Planet. Sci. (2017), 10.1016/j.proeps.2017.01.046

Arora et al., 2013

B. Arora, B.P. Mohanty, J.T. McGuire, I.M. Cozzarelli **Temporal dynamics of biogeochemical processes at the Norman Landfill site**

Water Resour. Res., 49 (2013), pp. 6909-6926, 10.1002/wrcr.20484

Arora et al., 2016a

B. Arora, D. Dwivedi, S.S. Hubbard, C.I. Steefel, K.H. Williams **Identifying geochemical hot moments and their controls on a contaminated river floodplain system using wavelet and entropy approaches**

Environ. Model. Softw., 85 (2016), pp. 27-41, 10.1016/j.envsoft.2016.08.005

Arora et al., 2016b

B. Arora, N.F. Splycher, C.I. Steefel, S. Molins, M. Bill, M.E. Conrad, W. Dong, B. Faybishenko, T.K. Tokunaga, J. Wan, K.H. Williams, S.B. Yabusaki **Influence of hydrological, biogeochemical and temperature transients on subsurface carbon fluxes in a flood plain environment**

Biogeochemistry, 127 (2016), pp. 367-396, 10.1007/s10533-016-0186-8

Atchley et al., 2016

A.L. Atchley, E.T. Coon, S.L. Painter, D.R. Harp, C.J. Wilson **Influences and interactions of inundation, peat, and snow on active layer thickness**

Geophys. Res. Lett., 43 (2016), pp. 5116-5123, 10.1002/2016GL068550

Balzter et al., 2015

H. Balzter, N. Tate, J. Kaduk, D. Harper, S. Page, R. Morrison, M. Muskulus, P. Jones **Multi-scale entropy analysis as a method for time-series analysis of climate data**

Climate, 3 (2015), pp. 227-240, 10.3390/cli3010227

Bastviken et al., 2004

D. Bastviken, J. Cole, M. Pace, L. Tranvik **Methane emissions from lakes: dependence of lake characteristics, two regional assessments, and a global estimate**

Glob. Biogeochem. Cycles, 18 (2004), 10.1029/2004GB002238

Battiti, 1994

R. Battiti **Using mutual information for selecting features in supervised neural net learning**

IEEE Trans. Neural Netw., 5 (1994), pp. 537-550, 10.1109/72.298224

Billings et al., 1982

W.D. Billings, J.O. Luken, D.A. Mortensen, K.M. Peterson **Arctic tundra: a source or sink for atmospheric carbon dioxide in a changing environment?**

Oecologia, 53 (1982), pp. 7-11, 10.1007/BF00377129

Bousquet et al., 2006

P. Bousquet, P. Ciais, J.B. Miller, E.J. Dlugokencky, D.A. Hauglustaine, C. Prigent, G.R. Van der Werf, P. Peylin, E.-G. Brunke, C. Carouge, R.L. Langenfelds, J. Lathière, F. Papa, M. Ramonet, M. Schmidt, L.P. Steele, S.C. Tyler, J. White **Contribution of anthropogenic and natural sources to atmospheric methane variability**

Nature, 443 (2006), pp. 439-443, 10.1038/nature05132

Brunsell and Wilson, 2013

N. Brunsell, C. Wilson **Multiscale interactions between water and carbon fluxes and environmental variables in a central U.S. grassland**

Entropy, 15 (2013), pp. 1324-1341, 10.3390/e15041324

Brunsell et al., 2008

N.A. Brunsell, J.M. Ham, C.E. Owensby **Assessing the multi-resolution information content of remotely sensed variables and elevation for evapotranspiration in a tall-grass prairie environment**

Remote Sens. Environ., 112 (2008), pp. 2977-2987, 10.1016/j.rse.2008.02.002

Bubier et al., 2003

J.L. Bubier, G. Bhatia, T.R. Moore, N.T. Roulet, Peter M. Lafleur **Spatial and temporal variability in growing-season net ecosystem carbon dioxide exchange at a large peatland in Ontario, Canada**

Ecosystems, 6 (2003), pp. 353-367, 10.1007/s10021-003-0125-0

Chapin et al., 2005

F.S. Chapin, M. Sturm, M.C. Serreze, J.P. McFadden, J.R. Key, A.H. Lloyd, A.D. McGuire, T.S. Rupp, A.H. Lynch, J.P. Schimel, J. Beringer, W.L. Chapman, H.E. Epstein, E.S. Euskirchen, L.D. Hinzman, G. Jia, C.L. Ping, K.D. Tape, C.D.C. Thompson, D.A. Walker, J.M. Welker **Role of land-surface changes in arctic summer warming**

Science, 310 (80) (2005), pp. 657-660, 10.1126/science.1117368

Costa et al., 2002

M. Costa, A. Goldberger, C.-K. Peng **Multiscale entropy analysis of complex physiologic time series**

Phys. Rev. Lett., 89 (2002), Article 068102, 10.1103/PhysRevLett.89.068102  
Cox et al., 2017

C.J. Cox, R.S. Stone, D.C. Douglas, D.M. Stanitski, G.J. Divoky, G.S. Dutton, C. Sweeney, J.C. George, D.U. Longenecker, C.J. Cox, R.S. Stone, D.C. Douglas, D.M. Stanitski, G.J. Divoky, G.S. Dutton, C. Sweeney, J.C. George, D.U. Longenecker **Drivers and environmental responses to the changing annual snow cycle of Northern Alaska**

Bull. Am. Meteorol. Soc., 98 (2017), pp. 2559-2577, 10.1175/BAMS-D-16-0201.1

Dafflon et al., 2016

B. Dafflon, S. Hubbard, C. Ulrich, J. Peterson, Y. Wu, H. Wainwright, T.J. Kneafsey **Geophysical estimation of shallow permafrost distribution and properties in an ice-wedge polygon-dominated Arctic tundra region**

Geophysics, 81 (2016), pp. WA247-WA263, 10.1190/geo2015-0175.1

Dafflon et al., 2017

B. Dafflon, R. Oktem, J. Peterson, C. Ulrich, A.P. Tran, S.S. Hubbard, V. Romanovsky, S.S. Hubbard **Coincident aboveground and belowground autonomous monitoring to quantify covariability in permafrost, soil, and vegetation properties in Arctic tundra**

J. Geophys. Res. Biogeosci., 122 (2017), pp. 1321-1342, 10.1002/2016JG003724

Davidson et al., 2016

S.J. Davidson, V.L. Sloan, G.K. Phoenix, R. Wagner, J.P. Fisher, W.C. Oechel, D. Zona **Vegetation type dominates the spatial variability in CH<sub>4</sub> emissions across multiple Arctic tundra landscapes**

Ecosystems, 19 (2016), pp. 1116-1132, 10.1007/s10021-016-9991-0

Dwivedi, 2012

D. Dwivedi **Texas Water Resources: Vulnerability from Contaminants**

Texas A&M University (2012)

Dwivedi and Mohanty, 2016

D. Dwivedi, B. Mohanty **Hot spots and persistence of nitrate in aquifers across scales**

Entropy, 18 (2016), p. 25, 10.3390/e18010025

Dwivedi et al., 2013

D. Dwivedi, B.P. Mohanty, B.J. Lesikar **Estimating Escherichia coli loads in streams based on various physical, chemical, and biological factors**

Water Resour. Res., 49 (2013), pp. 2896-2906, 10.1002/wrcr.20265

Dwivedi et al., 2016

D. Dwivedi, B.P. Mohanty, B.J. Lesikar **Impact of the Linked Surface Water-Soil Water-Groundwater System on Transport of E. coli in the Subsurface**

Water, Air, Soil Pollut. (2016), 10.1007/s11270-016-3053-2

Engstrom et al., 2005

R. Engstrom, A. Hope, H. Kwon, D. Stow, D. Zamolodchikov **Spatial distribution of near surface soil moisture and its relationship to microtopography in the Alaskan Arctic coastal plain**

Hydrol. Res., 36 (2005)

von Fischer et al., 2010

J.C. von Fischer, R.C. Rhew, G.M. Ames, B.K. Fossdick, P.E. von Fischer **Vegetation height and other controls of spatial variability in methane emissions from the Arctic coastal tundra at Barrow, Alaska**

J. Geophys. Res., 115 (2010), Article G00I03, 10.1029/2009JG001283

Friborg et al., 2000

T. Friborg, T.R. Christensen, B.U. Hansen, C. Nordstroem, H. Soegaard **Trace gas exchange in a high-Arctic valley: 2. Landscape CH<sub>4</sub> fluxes measured and modeled using eddy correlation data**

Glob. Biogeochem. Cycles, 14 (2000), pp. 715-723, 10.1029/1999GB001136

Gamon et al., 2012

J. a Gamon, G.P. Kershaw, S. Williamson, D.S. Hik **Microtopographic patterns in an arctic baydjarakh field: do fine-grain patterns enforce landscape stability?**

Environ. Res. Lett., 7 (2012), Article 015502, 10.1088/1748-9326/7/1/015502

Gangodagamage et al., 2014

C. Gangodagamage, J. Rowland, S. Hubbard, S. Brumby, A.K. Liljedahl, H. Wainwright, C.J. Wilson, G.L. Altmann, B. Dafflon, J. Peterson, C. Ulrich, C. Tweedie, S. Wullschleger **Extrapolating active layer thickness measurements across Arctic polygonal terrain using LiDAR and NDVI data sets**

Water Resour. Res., 50 (2014), pp. 6339-6357, 10.1002/2013WR014283. Received

Gaur and Mohanty, 2013

N. Gaur, B.P. Mohanty **Evolution of physical controls for soil moisture in humid and subhumid watersheds**



Water Resour. Res., 49 (2013), pp. 1244-1258, 10.1002/wrcr.20069

Grant et al., 2017

R.F. Grant, Z.A. Mekonnen, W.J. Riley, B. Arora, M.S. Torn **Mathematical modelling of Arctic polygonal tundra with Ecosys: 2. Microtopography determines how CO<sub>2</sub> and CH<sub>4</sub> exchange responds to changes in temperature and precipitation**

J. Geophys. Res. Biogeosci., 122 (2017), pp. 3174-3187, 10.1002/2017JG004037

Grogan and Chapin III, 1999

P. Grogan, F.S. Chapin III **Arctic soil respiration: effects of climate and vegetation depend on season**

Ecosystems, 2 (1999), pp. 451-459, 10.1007/s100219900093

Harp et al., 2016

D.R. Harp, A.L. Atchley, S.L. Painter, E.T. Coon, C.J. Wilson, V.E. Romanovsky, J.C. Rowland **Effect of soil property uncertainties on permafrost thaw projections: a calibration-constrained analysis**

Cryosphere, 10 (2016), pp. 341-358, 10.5194/tc-10-341-2016

Harper et al., 2005

C.W. Harper, J.M. Blair, P.A. Fay, A.K. Knapp, J.D. Carlisle **Increased rainfall variability and reduced rainfall amount decreases soil CO<sub>2</sub> flux in a grassland ecosystem**

Glob. Chang. Biol., 11 (2005), pp. 322-334, 10.1111/j.1365-2486.2005.00899.x

Helbig et al., 2013

M. Helbig, J. Boike, M. Langer, P. Schreiber, B.R.K. Runkle, L. Kutzbach **Spatial and seasonal variability of polygonal tundra water balance: Lena River Delta, northern Siberia (Russia)**

Hydrogeol. J., 21 (2013), pp. 133-147, 10.1007/s10040-012-0933-4

Herndon et al., 2015

E.M. Herndon, Z. Yang, J. Bargar, N. Janot, T.Z. Regier, D.E. Graham, S.D. Wulfschleger, B. Gu, L. Liang **Geochemical drivers of organic matter decomposition in Arctic tundra soils**

Biogeochemistry, 126 (2015), pp. 397-414, 10.1007/s10533-015-0165-5

Hinkel and Nelson, 2003

K.M. Hinkel, F.E. Nelson **Spatial and temporal patterns of active layer thickness at circumpolar active layer monitoring (CALM) sites in northern Alaska, 1995-2000**

J. Geophys. Res., 108 (2003), p. 8168, 10.1029/2001JD000927

Hinkel et al., 2003

K.M. Hinkel, W.R. Eisner, J.G. Bockheim, F.E. Nelson, K.M. Peterson, X. Dai **Spatial extent, age, and carbon stocks in drained thaw Lake basins on the barrow Peninsula, Alaska. Arctic**

Antarct. Alp. Res., 35 (2003), pp. 291-300, 10.1657/1523-0430(2003)035[0291:SEAACS]2.0.CO;2

Hubbard et al., 2013

S.S. Hubbard, C. Gangodagamage, B. Dafflon, H. Wainwright, J. Peterson, A. Gusmeroli, C. Ulrich, Y. Wu, C. Wilson, J. Rowland, C. Tweedie, S.D. Wulschleger **Quantifying and relating land-surface and subsurface variability in permafrost environments using LiDAR and surface geophysical datasets**

Hydrogeol. J., 21 (2013), pp. 149-169, 10.1007/s10040-012-0939-y

IPCC, 2013

IPCC **Summary for policymakers**

T.F. Stocker, D. Qin, G.-K. Plattner, M. Tignor, S.K. Allen, J. Boschung, A. Nauels, Y. Xia, V. Bex, P.M. Midgley (Eds.), Climate Change 2013: The Physical Science Basis. Contribution of Working Group I to the Fifth Assessment Report of the Intergovernmental Panel on Climate Change, Cambridge University Press, Cambridge and New York (2013)

Janssens et al., 2001

I.A. Janssens, H. Lankreijer, G. Matteucci, A.S. Kowalski, N. Buchmann, D. Epron, K. Pilegaard, W. Kutsch, B. Longdoz, T. Grunwald, L. Montagnani, S. Dore, C. Rebmann, E.J. Moors, A. Grelle, U. Rannik, K. Morgenstern, S. Oltchev, R. Clement, J. Gudmundsson, S. Minerbi, P. Berbigier, A. Ibrom, J. Moncrieff, M. Aubinet, C. Bernhofer, N.O. Jensen, T. Vesala, A. Granier, E.-D. Schulze, A. Lindroth, A.J. Dolman, P.G. Jarvis, R. Ceulemans, R. Valentini

**Productivity overshadows temperature in determining soil and ecosystem respiration across European forests**

Glob. Chang. Biol., 7 (2001), pp. 269-278, 10.1046/j.1365-2486.2001.00412.x

Juszk et al., 2016

I. Juszk, W. Eugster, M.M.P.D. Heijmans, G. Schaepman-Strub **Contrasting radiation and soil heat fluxes in Arctic shrub and wet sedge tundra**

Biogeosciences, 13 (2016), pp. 4049-4064, 10.5194/bg-13-4049-2016

Kawachi et al., 2001

T. Kawachi, T. Maruyama, V.P. Singh **Rainfall entropy for delineation of water resources zones in Japan**

J. Hydrol., 246 (2001), pp. 36-44, 10.1016/S0022-1694(01)00355-9

Kruskal and Wallis, 1952

W.H. Kruskal, W.A. Wallis **Use of ranks in one-criterion variance analysis**

J. Am. Stat. Assoc., 47 (1952), pp. 583-621,  
10.1080/01621459.1952.10483441

Kumar et al., 2016

J. Kumar, N. Collier, G. Bisht, R.T. Mills, P.E. Thornton, C.M. Iversen, V. Romanovsky **Modeling the spatiotemporal variability in subsurface thermal regimes across a low-relief polygonal tundra landscape**

Cryosphere, 10 (2016), pp. 2241-2274, 10.5194/tc-10-2241-2016

Lachenbruch and Marshall, 1986

A.H. Lachenbruch, B.V. Marshall **Changing climate: geothermal evidence from permafrost in the Alaskan Arctic**

Science, 234 (80) (1986), pp. 689-696, 10.1126/science.234.4777.689

Lara et al., 2015

M.J. Lara, A.D. Mcguire, E.S. Euskirchen, C.E. Tweedie, K.M. Hinkel, A.N. Skurikhin, V.E. Romanovsky, G. Grosse, W.R. Bolton, H. Genet **Polygonal tundra geomorphological change in response to warming alters future CO<sub>2</sub> and CH<sub>4</sub> flux on the Barrow Peninsula**

Glob. Chang. Biol., 21 (2015), pp. 1634-1651, 10.1111/gcb.12757

Lawrence et al., 2015

D. Lawrence, C. Koven, S. Swenson, W. Riley, A. Slater **Permafrost thaw and resulting soil moisture changes regulate projected high-latitude CO<sub>2</sub> and CH<sub>4</sub> emissions**

Environ. Res. Lett., 10 (2015), Article 094011, 10.1088/1748-9326/10/9/094011

Leffingwell, 1915

E. de K. Leffingwell **Ground-ice wedges: the dominant form of ground-ice on the north coast of Alaska on JSTOR**

J. Geol., 23 (1915), pp. 635-654

Liljedahl et al., 2011

A.K. Liljedahl, L.D. Hinzman, Y. Harazono, D. Zona, C.E. Tweedie, R.D. Hollister, R. Engstrom, W.C. Oechel **Nonlinear controls on evapotranspiration in arctic coastal wetlands**

Biogeosciences, 8 (2011), pp. 3375-3389, 10.5194/bg-8-3375-2011

Liljedahl et al., 2012

A.K. Liljedahl, L.D. Hinzman, J. Schulla **Ice-wedge polygon type controls low-gradient watershed-scale hydrology**

K.M. Hinkel (Ed.), Tenth International Conference on Permafrost, The Northern Publisher, Salekhard, Russia (2012), pp. 231-236

Liljedahl et al., 2016

A.K. Liljedahl, J. Boike, R.P. Daanen, A.N. Fedorov, G.V. Frost, G. Grosse, L.D. Hinzman, Y. Iijima, J.C. Jorgenson, N. Matveyeva, M. Necsoiu, M.K. Reynolds, V.E. Romanovsky, J. Schulla, K.D. Tape, D.A. Walker, C.J. Wilson, H. Yabuki, D. Zona **Pan-Arctic ice-wedge degradation in warming permafrost and its influence on tundra hydrology**

Nat. Geosci., 9 (2016), pp. 312-318, 10.1038/ngeo2674

Liston et al., 2002

G.E. Liston, J.P. McFadden, M. Sturm, R.A. Pielke **Modelled changes in Arctic tundra snow, energy and moisture fluxes due to increased shrubs**

Glob. Chang. Biol., 8 (2002), pp. 17-32, 10.1046/j.1354-1013.2001.00416.x

MacKay, 2000

J.R. MacKay **Thermally induced movements in ice-wedge polygons, western arctic coast: a long-term study**

Géograph. Phys. Quat., 54 (2000), p. 41, 10.7202/004846ar

Malhotra and Roulet, 2015

A. Malhotra, N.T. Roulet **Environmental correlates of peatland carbon fluxes in a thawing landscape: do transitional thaw stages matter?**

Biogeosciences, 12 (2015), pp. 3119-3130, 10.5194/bg-12-3119-2015

Mann and Whitney, 1947

H.B. Mann, D.R. Whitney **On a test of whether one of two random variables is stochastically larger than the other**

Ann. Math. Stat. (1947), 10.2307/2236101

Mastepanov et al., 2013

M. Mastepanov, C. Sigsgaard, T. Tagesson, L. Ström, M.P. Tamstorf, M. Lund, T.R. Christensen **Revisiting factors controlling methane emissions from high-Arctic tundra**

Biogeosciences, 10 (2013), pp. 5139-5158, 10.5194/bg-10-5139-2013

Matejka and Fitzmaurice, 2017

J. Matejka, G. Fitzmaurice **Same stats, different graphs**

Proceedings of the 2017 CHI Conference on Human Factors in Computing Systems - CHI '17, ACM Press, New York, New York, USA (2017), pp. 1290-1294, 10.1145/3025453.3025912

Mauritz et al., 2017

M. Mauritz, R. Bracho, G. Celis, J. Hutchings, S.M. Natali, E. Pegoraro, V.G. Salmon, C.Schädel, E.E. Webb, E.A.G. Schuur **Nonlinear CO<sub>2</sub> flux response to 7 years of experimentally induced permafrost thaw**

Glob. Chang. Biol., 23 (2017), pp. 3646-3666, 10.1111/gcb.13661

Minke et al., 2009

M. Minke, N. Donner, N.S. Karpov, P. de Klerk, H. Joosten **Patterns in vegetation composition, surface height and thaw depth in polygon mires in the Yakutian Arctic (NE Siberia): a microtopographical characterisation of the active layer**

Permafr. Periglac. Process., 20 (2009), pp. 357-368

Mogheir et al., 2004

Y. Mogheir, J.L.M.P. de Lima, V.P. Singh **Characterizing the spatial variability of groundwater quality using the entropy theory: II. Case study from Gaza strip**

Hydrol. Process., 18 (2004), pp. 2579-2590, 10.1002/hyp.1466

Myneni et al., 1997

R.B. Myneni, C.D. Keeling, C.J. Tucker, G. Asrar, R.R. Nemani **Increased plant growth in the northern high latitudes from 1981 to 1991**

Nature, 386 (1997), pp. 698-702, 10.1038/386698a0

Newman et al., 2015

B.D. Newman, H.M. Throckmorton, D.E. Graham, B. Gu, S.S. Hubbard, L. Liang, Y. Wu, J.M. Heikoop, E.M. Herndon, T.J. Phelps, C.J. Wilson, S.D. Wulfschleger **Microtopographic and depth controls on active layer chemistry in Arctic polygonal ground**

Geophys. Res. Lett., 42 (2015), pp. 1808-1817, 10.1002/2014GL062804

Oberbauer et al., 2007

S.F. Oberbauer, C.E. Tweedie, J.M. Welker, J.T. Fahnestock, G.H.R. Henry, P.J. Webber, R.D. Hollister, M.D. Walker, A. Kuchy, E. Elmore, G. Starr **Tundra CO<sub>2</sub> fluxes in response to experimental warming across latitudinal and moisture gradients**

Ecol. Monogr., 77 (2007), pp. 221-238, 10.1890/06-0649

Oechel et al., 1995

W.C. Oechel, G.L. Vourlitis, S.J. Hastings, S.A. Bochkarev **Change in Arctic CO<sub>2</sub> flux over two decades: effects of climate change at Barrow, Alaska**

Ecol. Appl., 5 (1995), pp. 846-855, 10.2307/1941992

Oechel et al., 2000

W.C. Oechel, G.L. Vourlitis, S.J. Hastings, R.C. Zulueta, L. Hinzman, D. Kane **Acclimation of ecosystem CO<sub>2</sub> exchange in the Alaskan Arctic in response to decadal climate warming**

Nature, 406 (2000), pp. 978-981, 10.1038/35023137

Rajsekhar et al., 2012

D. Rajsekhar, A. Mishra, V. Singh **Regionalization of drought characteristics using an entropy approach**

J. Hydrol. Eng., 18 (2012), pp. 870-887, 10.1061/(ASCE)HE.1943-5584.0000683

Raz-Yaseef et al., 2017

N. Raz-Yaseef, M.S. Torn, Y. Wu, D.P. Billesbach, A.K. Liljedahl, T.J. Kneafsey, V.E. Romanovsky, D.R. Cook, S.D. Wullschleger **Large CO<sub>2</sub> and CH<sub>4</sub> emissions from polygonal tundra during spring thaw in northern Alaska**

Geophys. Res. Lett., 44 (2017), pp. 504-513, 10.1002/2016GL071220

Reimann and Filzmoser, 2000

C. Reimann, P. Filzmoser **Normal and lognormal data distribution in geochemistry: death of a myth. Consequences for the statistical treatment of geochemical and environmental data**

Environ. Geol., 39 (2000), pp. 1001-1014, 10.1007/s002549900081

Ruddell et al., 2013

B.L. Ruddell, N.A. Brunsell, P. Stoy **Applying information theory in the geosciences to quantify process uncertainty, feedback, scale**

EOS Trans. Am. Geophys. Union, 94 (2013), p. 56, 10.1002/2013EO050007

Sachs et al., 2008

T. Sachs, C. Wille, J. Boike, L. Kutzbach **Environmental controls on ecosystem-scale CH<sub>4</sub> emission from polygonal tundra in the Lena River Delta, Siberia**

J. Geophys. Res., 113 (2008), Article G00A03, 10.1029/2007JG000505

Schimel et al., 2001

D.S. Schimel, J.I. House, K.A. Hibbard, P. Bousquet, P. Ciais, P. Peylin, B.H. Braswell, M.J. Apps, D. Baker, A. Bondeau, J. Canadell, G. Churkina, W.

Cramer, A.S. Denning, C.B. Field, P.Friedlingstein, C. Goodale, M. Heimann, R.A. Houghton, J.M. Melillo, B. Moore, D. Murdiyarso, I. Noble, S.W. Pacala, I.C. Prentice, M.R. Raupach, P.J. Rayner, R.J. Scholes, W.L. Steffen, C. Wirth**Recent patterns and mechanisms of carbon exchange by terrestrial ecosystems**

Nature, 414 (2001), pp. 169-172, 10.1038/35102500

Scott, 1979

D.W. Scott**On optimal and data-based histograms**

Biometrika, 66 (1979), pp. 605-610, 10.1093/biomet/66.3.605

Sellman et al., 1975

P.V. Sellman, J. Brown, R.I. Lewellen, H. McKim, C. Merry**The Classification and Geomorphic Implication of Thaw Lakes on the Arctic Coastal Plain**

(1975)

(Hanover, New Hampshire)

Shannon, 1948a

C.E. Shannon**A mathematical theory of communication, I and II**

Bell Syst. Tech. J., 27 (1948), pp. 379-443, 10.1145/584091.584093

Shannon, 1948b

C.E. Shannon**A mathematical theory of communication, III-V**

Bell Syst. Tech. J., 27 (1948), pp. 623-656

Sharratt, 1992

B. Sharratt**Growing season trends in the Alaskan climate record**

Arctic, 45 (1992), pp. 124-127

Shiklomanov et al., 2010

N.I. Shiklomanov, D.A. Streletskiy, F.E. Nelson, R.D. Hollister, V.E. Romanovsky, C.E. Tweedie, J.G. Bockheim, J. Brown**Decadal variations of active-layer thickness in moisture-controlled landscapes, Barrow, Alaska**

J. Geophys. Res., 115 (2010), Article G00I04, 10.1029/2009JG001248

Sileshi, 2014

G.W. Sileshi**A critical review of forest biomass estimation models, common mistakes and corrective measures**

For. Ecol. Manag., 329 (2014), pp. 237-254, 10.1016/j.FORECO.2014.06.026

Singh, 1997

V.P. Singh **The use of entropy in hydrology and water resources**

Hydrol. Process., 11 (1997), pp. 587-626

Singh, 2013

V.P. Singh **Entropy theory**

Entropy Theory and its Application in Environmental and Water Engineering, John Wiley & Sons, Ltd(2013), pp. 33-141

Sistla et al., 2013

S.A. Sistla, J.C. Moore, R.T. Simpson, L. Gough, G.R. Shaver, J.P.

Schimel **Long-term warming restructures Arctic tundra without changing net soil carbon storage**

Nature, 497 (2013), pp. 615-618, 10.1038/nature12129

Stow et al., 2004

D.A. Stow, A. Hope, D. McGuire, D. Verbyla, J. Gamon, F. Huemmrich, S. Houston, C. Racine, M. Sturm, K. Tape, L. Hinzman, K. Yoshikawa, C. Tweedie, B. Noyle, C. Silapaswan, D. Douglas, B. Griffith, G. Jia, H. Epstein, D. Walker, S. Daeschner, A. Petersen, L. Zhou, R. Myneni **Remote sensing of vegetation and land-cover change in Arctic tundra ecosystems**

Remote Sens. Environ., 89 (2004), pp. 281-308, 10.1016/j.rse.2003.10.018

Street et al., 2007

L.E. Street, G.R. Shaver, M. Williams, M.T. Van Wijk **What is the relationship between changes in canopy leaf area and changes in photosynthetic CO<sub>2</sub> flux in arctic ecosystems?**

J. Ecol., 95 (2007), pp. 139-150, 10.1111/j.1365-2745.2006.01187.x

Strehl et al., 2000

A. Strehl, J. Ghosh, R. Mooney **Impact of similarity measures on web-page clustering**

Workshop on Artificial Intelligence for Web Search (2000), pp. 58-64

Austin. (doi:10.1.1.29.2377)

Sturtevant et al., 2012

C.S. Sturtevant, W.C. Oechel, D. Zona, Y. Kim, C.E. Emerson **Soil moisture control over autumn season methane flux, Arctic Coastal Plain of Alaska**

Biogeosciences, 9 (2012), pp. 1423-1440, 10.5194/bg-9-1423-2012

Subke and Bahn, 2010

J.-A. Subke, M. Bahn **On the “temperature sensitivity” of soil respiration: can we use the immeasurable to predict the unknown?**



Soil Biol. Biochem., 42 (2010), pp. 1653-1656, 10.1016/j.soilbio.2010.05.026

Torn et al., 2013

M.S. Torn, M.S. Hahn, J.B. Curtis, V.L. Sloan, O. Chafe **CO<sub>2</sub> and CH<sub>4</sub> Surface Flux, Air Temperature, Soil Temperature and Soil Moisture, Barrow, Alaska, 2013, Ver. 1**

Oak Ridge, TN

(2013), 10.5440/1167255

Tucker et al., 2001

C.J. Tucker, D.A. Slayback, J.E. Pinzon, S.O. Los, R.B. Myneni, M.G.

Taylor **Higher northern latitude normalized difference vegetation index and growing season trends from 1982 to 1999**

Int. J. Biometeorol., 45 (2001), pp. 184-190, 10.1007/s00484-001-0109-8

Vaughn and Torn, 2018

L. Vaughn, M. Torn **Radiocarbon in CO<sub>2</sub> and Soil Organic Matter from Laboratory Incubations, Barrow, Alaska, 2012. Next Generation Ecosystem Experiments Arctic Data Collection, Oak Ridge National Laboratory**

U.S. Department of Energy, Oak Ridge, Tennessee, USA (2018), 10.5440/1418852

Vaughn et al., 2016

L.J.S. Vaughn, M.E. Conrad, M. Bill, M.S. Torn **Isotopic insights into methane production, oxidation, and emissions in Arctic polygon tundra**

Glob. Chang. Biol., 22 (2016), pp. 3487-3502, 10.1111/gcb.13281

Wainwright et al., 2015

H.M. Wainwright, B. Dafflon, L.J. Smith, M.S. Hahn, J.B. Curtis, Y. Wu, C. Ulrich, J.E. Peterson, M.S. Torn, S.S. Hubbard **Identifying multiscale zonation and assessing the relative importance of polygon geomorphology on carbon fluxes in an Arctic tundra ecosystem**

J. Geophys. Res. Biogeosci., 120 (2015), pp. 788-808, 10.1002/2014JG002799

Wainwright et al., 2016

H.M. Wainwright, A.K. Liljedahl, B. Dafflon, C. Ulrich, J.E. Peterson, S.S. Hubbard **Mapping snow depth within a tundra ecosystem using multiscale observations and Bayesian methods**

Cryosphere Discuss. (2016), pp. 1-56, 10.5194/tc-2016-168

Walker et al., 2008

D.A. Walker, H.E. Epstein, V.E. Romanovsky, C.L. Ping, G.J. Michaelson, R.P. Daanen, Y. Shur, R.A. Peterson, W.B. Krantz, M.K. Reynolds, W.A. Gould, G. Gonzalez, D.J. Nicolsky, C.M. Vonlanthen, A.N. Kade, P. Kuss, A.M. Kelley, C.A. Munger, C.T. Tarnocai, N.V. Matveyeva, F.J.A. Daniëls **Arctic patterned-ground ecosystems: a synthesis of field studies and models along a North American Arctic transect**

J. Geophys. Res., 113 (2008), Article G03S01, 10.1029/2007JG000504

Walter et al., 2007

K.M. Walter, L.C. Smith, F.S. Chapin **Methane bubbling from northern lakes: present and future contributions to the global methane budget**

Philos. Trans. A. Math. Phys. Eng. Sci., 365 (2007), pp. 1657-1676, 10.1098/rsta.2007.2036

Xu et al., 2006

L. Xu, M.D. Furtaw, R.A. Madsen, R.L. Garcia, D.J. Anderson, D.K. McDermitt **On maintaining pressure equilibrium between a soil CO<sub>2</sub> flux chamber and the ambient air**

J. Geophys. Res., 111 (2006), Article D08S10, 10.1029/2005JD006435

Yabusaki et al., 2017

S.B. Yabusaki, M.J. Wilkins, Y. Fang, K.H. Williams, B. Arora, J. Bargar, H.R. Beller, N.J. Bouskill, E.L. Brodie, J.N. Christensen, M.E. Conrad, R.E. Danczak, E. King, M.R. Soltanian, N.F. Spycher, C.I. Steefel, T.K. Tokunaga, R. Versteeg, S.R. Waichler, H.M. Wainwright **Water table dynamics and biogeochemical cycling in a shallow variably-saturated floodplain**

Environ. Sci. Technol. (2017), 10.1021/acs.est.6b04873

Zona et al., 2009

D. Zona, W.C. Oechel, J. Kochendorfer, U.K.T. Paw, A.N. Salyuk, P.C. Olivas, S.F. Oberbauer, D.A. Lipson **Methane fluxes during the initiation of a large-scale water table manipulation experiment in the Alaskan Arctic tundra**

Glob. Biogeochem. Cycles, 23 (2009), 10.1029/2009GB003487

Zona et al., 2011

D. Zona, D.A. Lipson, R.C. Zulueta, S.F. Oberbauer, W.C. Oechel **Microtopographic controls on ecosystem functioning in the Arctic Coastal Plain**

J. Geophys. Res., 116 (2011), Article G00I08, 10.1029/2009JG001241

Zona et al., 2016

D. Zona, B. Gioli, R. Commane, J. Lindaas, S.C. Wofsy, C.E. Miller, S.J. Dinardo, S. Dengel, C. Sweeney, A. Karion, R.Y.-W. Chang, J.M. Henderson, P.C. Murphy, J.P. Goodrich, V. Moreaux, A. Liljedahl, J.D. Watts, J.S. Kimball, D.A. Lipson, W.C. Oechel **Cold season emissions dominate the Arctic tundra methane budget**

Proc. Natl. Acad. Sci. U. S. A., 113 (2016), pp. 40-45,  
10.1073/pnas.1516017113

$$H = - \sum_{i=1}^B P_i \log_2(P_i) \quad (1)$$

where,  $B$  is the set of measurements and  $P_i$  denotes the probability of outcome as  $i$  varies from 1 to  $B$ . Using the histogram bin width based on Scott's choice method (Scott, 1979), the discrete data interval  $i$  was determined. Eq. (1) suggests that the value of entropy varies according to the distribution of  $P_i$ 's associated with the set  $B$  chosen to represent the random variable. This implies that by increasing the number of constraints, or by specifying more information about the random variable, the range of entropy decreases. Therefore, process components that add information to the system reduce Shannon's entropy and are able to explain the variability in the data series. This concept forms the basis of our study.

Eq. (1) further indicates that there is no upper bound for entropy because if any  $P_i$  tends to 0,  $\log(\cdot)$  will tend to infinity. Therefore, we normalize entropy as (Dwivedi, 2012):

$$H_N = \frac{\max(H) - H}{\max(H)} \times 100; \quad (2)$$

such that the normalized marginal entropy ( $H_N$ ) varies between 0 and 100. Entropy is maximum when all events are equally probable and all  $P_{i_s}$  are equal, such that.

$$\max(H) = - \sum_{i=1}^B \frac{1}{B} \log_2 \left( \frac{1}{B} \right) = \log_2(B) \quad (3)$$

Thus,

$$D = T_N(V, F^c) - H_{N,year} \quad (5)$$